Changes in glacier equilibrium-line altitude in the western Alps from 1984 to 2010: evaluation by remote sensing and modeling of the morpho-topographic and climate controls

Antoine Rabatel[(1)], Anne Letréguilly[(1)], Jean-Pierre Dedieu[(2)], Nicolas Eckert[(3)]

[(1)] Univ. Grenoble Alpes, CNRS, LGGE (UMR5183), F-38000 Grenoble, France.

[(2)] Univ. Grenoble Alpes, CNRS, IRD, LTHE (UMR5564), F-38000 Grenoble, France.

[(3)] IRSTEA, UR ETGR F-38000 Grenoble, France.

Corresponding author:

Dr. Antoine Rabatel

Laboratoire de Glaciologie et Géophysique de l'Environnement

54, rue Molière

38400 Saint Martin d'Hères, FRANCE

Tel : 00 33 4 76 82 42 71

Fax : 00 33 4 76 82 42 01

antoine.rabatel@ujf-grenoble.fr

Abstract

We present time series of equilibrium-line altitude (ELA) measured from the end-of-summer snowline altitude computed using satellite images, for 43 glaciers in the western Alps over the 1984-2010 period. More than 120 satellite images acquired by Landsat, SPOT and ASTER were used. In parallel, changes in climate variables (summer cumulative positive degree days, CPDD, and winter precipitation) were analyzed over the same time period using 22 weather stations located inside and around the study area. Assuming a continuous linear trend over the study period: (1) the average ELA of the 43 glaciers increased by about 170 m; (2) summer CPDD increased by about 150 PDD at 3000 m a.s.l.; and (3) winter precipitation remained rather stationary. Summer CPDD showed homogeneous spatial and temporal variability; winter precipitation showed homogeneous temporal variability, but some stations showed a slightly different spatial pattern. Regarding ELAs, temporal variability between the 43 glaciers was also homogeneous, but spatially, glaciers in the southern part of the study area differed from glaciers in the northern part, mainly due to a different precipitation pattern. A sensitivity analysis of the ELAs to climate and morpho-topographic variables (elevation, aspect, latitude) highlighted the following: (1) the average ELA over the study period of each glacier is strongly controlled by morpho-topographic variables; and (2) the interannual variability of the ELA is strongly controlled by climate variables, with the observed increasing trend mainly driven by increasing temperatures, even if significant nonlinear low frequency fluctuations appear to be driven by winter precipitation anomalies. Finally, we used an expansion of Lliboutry's approach to reconstruct fluctuations in the ELA of any glacier of the study area with respect to morpho-topographic and climate variables, by quantifying their respective weight and the related uncertainties in a consistent manner within a hierarchical Bayesian framework. This method was tested and validated using the ELA measured on the satellite images.

Key words: Glacier, Equilibrium-line altitude, Satellite remote-sensing, Climate sensitivity, Hierarchical variance decomposition model, Western European Alps

1. INTRODUCTION

Historically, the glacier's annual surface mass balance and equilibrium-line altitude (ELA) have been computed from direct field measurements of snow accumulation and snow/ice ablation through point measurements using a network of ablation stakes and snow pits on individual glaciers. The longest mass balance data series started in the late 1940s for Storglaciären (Sweden), Taku Glacier (USA), Limmern and Plattalva glaciers (Switzerland), Sarennes Glacier (France) and Storbreen (Norway). The World Glacier Monitoring Service (WGMS) has mass balance data on around 260 glaciers worldwide (note that the World Glacier Inventory contains more than 130,000 glaciers), but uninterrupted time series spanning more than 40 years are available for only 37 glaciers (WGMS, 2012). The small number of available data series is due to the cost, in terms of money, manpower, and time, of this laborious method. The small number of data series is an obstacle that needs to be overcome if we are to improve our knowledge of the relationship between climate and glacier changes at the scale a mountain range and up to regional scale, as well as our knowledge of the contribution of glaciers to water resources in the functioning of high-altitude watersheds. Remote sensing provides a unique opportunity to address the question of glacier changes at regional scale. Since the availability of satellite data in the 1970s, several methods have been developed to compute changes in glacier volume at multiannual to decadal scale using digital elevation models (DEMs) (e.g. Echelmeyer et al., 1996; Baltsavias et al., 1999; Berthier et al., 2004; Gardelle et al., 2012), or the annual ELA and mass balance (e.g. Østrem, 1975; Rabatel et al., 2005, 2008, 2012a). However, satellite derived DEMs are not accurate enough to compute variations in the annual volume of mountain glaciers. Another alternative emerged from recent studies based on ELA and distributed mass balance modeling using meteorological input fields derived from local weather stations, data reanalysis, or regional climate models (e.g. Zemp et al., 2007; Machguth et al., 2009; Marzeion et al., 2012). However, such modeling approaches still have a number of limitations, e.g. accumulation is underestimated in mountainous regions. On the other hand, for mid-latitude mountain glaciers, the end-of-summer snowline altitude (SLA) is a good indicator of the ELA and thus of the annual mass balance (Lliboutry, 1965; Braithwaite, 1984; Rabatel et al., 2005). This enables ELA changes to be reconstructed for long time periods from remote-sensing data (Demuth and Pietroniro, 1999; Rabatel

et al., 2002, 2005, 2008; Barcaza et al., 2009; Mathieu et al., 2009), because the snowline is generally easy to identify using aerial photographs and satellite images (Meier, 1980; Rees, 2005). Consequently, it is possible to study the climate-glacier relationship at a massif or regional scale (Clare et al., 2002; Chinn et al., 2005), which is particularly useful in remote areas where no direct measurements are available.

In the current study, we rely on previous studies conducted in the French Alps (Dedieu and Reynaud, 1990; Rabatel et al., 2002, 2005, 2008), to reconstruct ELA time series for more than 40 glaciers over the 1984-2010 period, using the end-of-summer snowline detected on satellite images. Our aim are: (1) to quantify at a regional scale the temporal and spatial changes of the ELA; (2) to characterize the relationships between ELA and both morpho-topographic and climate variables; and (3) to reconstruct the spatio-temporal variability of annual ELA time series by incorporating the above mentioned relationships in an expansion of Lliboutry's variance decomposition model (1974).

~~In Section 2 we describe the study area, and the data and methodologies used in the current work. In section 3, we detail temporal and spatial changes in each one of the variables: ELA, summer cumulative positive degree days and winter precipitation. In Section 4, we focus first on the relationship between the ELA and morpho-topograpic variables, and second, on the relationship between the ELA and climate variables. Finally, relying on the hierarchical framework proposed by Eckert et al. (2011) for mass balance point measurments, we incorporate these relationships in an expansion of Lliboutry's variance decomposition model (1974) to reconstruct the spatio-temporal variability of annual ELA time series. We compare and validate the modeled data with the ELA measured from satellite images.~~

2. STUDY AREA, DATA AND METHOD

2.1 Selection of the study sites

A recent update of the glacier inventory of the French Alps lists 593 glaciers (Rabatel et al., 2012b). The total glacial coverage in the French Alps was about 340 km² in the mid-1980s and had decreased to about 275 km² in the late 2000s. In the current study, 43 glaciers located in the French Alps or just next to border with Switzerland and Italy were selected (Table 1, Figure 1). The selection was based

on the following criteria: (1) glaciers had to have a high enough maximum elevation to allow observation of the snowline every year during the study period; (2) glaciers with all aspects had to be represented; and (3) glaciers located in all the glacierized mountain ranges in the French Alps from the southern-most (44°50' N) to the northern-most (46°00' N) had to be included.

Among the selected glaciers, three belong to the GLACIOCLIM observatory ~~(http://www-lgge.ujf-grenoble.fr/ServiceObs/index.htm)~~ which runs a permanent mass balance monitoring program. These three glaciers are Saint Sorlin Glacier, monitored since 1957 (# 31 in Table 1 and Fig. 1), Argentière Glacier monitored since 1975 (# 4 in Table 1 and Fig. 1), and Gébroulaz Glacier monitored since 1983 (# 28 in Table 1 and Fig. 1). Mass balance data available on these three glaciers were used to assess the representativity of the end-of-summer SLA computed from the satellite images as an indicator of the ELA and of the annual mass balance computed from field measurements (see section 3.1 below).

2.2. Snowline altitude retrieved from satellite images

2.2.1. Satellite images and snowline delineation

A total of 122 images of the 43 glaciers were used to cover the 27-year study period. Unfortunately, in some years usable images were not available for all the glaciers because of (1) cloud cover hiding the underlying terrain; and (2) snowfalls that can occur in late summer and completly cover the glaciers. This was mainly the case in the 1980s and 1990s when fewer satellites were in orbit than in the 2000s. The images we used were acquired by the following satellites: Landsat 4TM, 5TM, 7ETM+, SPOT 1 to 5 and ASTER, with spatial resolutions ranging from 2.5 to 30 m (see supplementary material: Table I for a detailed list of the images used).

For the snowline delineation on multispectral images, a test of band combinations and band ratios to facilitate the identification of the snowline on the images is described in Rabatel *et al.* (2012a, see Figure 4). These authors concluded that the combination of the green, near-infrared, and short-wave infrared bands (see Table 2 for details about the wavelengths of each satellite) was the most appropriate to identify the limit between snow and ice. The snowline was delineated on the central part of the glaciers to avoid border effects on the glacier banks (shadows from surrounding slopes, additional snow input by avalanches, over-accumulation due to wind) which could generate

equilibrium-line position dependence on local conditions (Rabatel *et al.*, 2005). The delineation has been performed manually because automatic method hardly succeed in distinguishing the snowline from the firn-line when both are presented on the glacier. A distinction which results to be also difficult visually when the pixel size of the satellite images is too coarse (see the discussion section).

2.2.2. Digital elevation model, computation of the altitude of the snowline and of the glacier morpho-topographic variables

To avoid border effects on the glacier banks (Figure 2), which could mean that the position of the snowline depended on local conditions (shadows from surrounding slopes, additional snow input due to avalanches or wind drift), the SLA was only measured on the central part of each glacier. The average altitude of each snowline was calculated by overlaying the shapefiles containing the digitized snowlines on a DEM. For each glacier, the DEM was also used to compute the following morpho-topographic variables used in this study: surface area, mean elevation, aspect, latitude and longitude of the glacier centroid. The mean elevation of each glacier has been computed as the arithmetic mean of the elevation of each pixel of the DEM included within the glaciers outline. This mean elevation is rather close to the median elevation of the glaciers. Indeed, the difference between the two variables is 10 m in average for the 43 studied glaciers. This shows that the studied glaciers have in average, an almost symmetrical area-altitude distribution (Braithwaite and Raper, 2010).

Several DEMs are available for the study area. Among these, one comes from the French National Geographical Institute (IGN) with a resolution of 25 m, and dates from the early 1980s. Another one is the ASTERGDEM with a resolution of 30 m, and dates from the mid-2000s. The average difference between the two DEMs at the mean elevation of the SLA of the 43 glaciers studied over the whole study period, i.e. approx. 3,050 m a.s.l., is about 20 m. This matches the vertical accuracy of the DEMs, and is small in comparison to the interannual variability of the SLA (the standard deviation of the measured SLA over the whole study period ranges between 75 and 255 m depending on the glacier). However, because the glacier surface lowering can reach several tens of meters at lower elevation (up to 60 m at 1,500 m a.s.l.) due to the important glacier shrinkage over the last decades (Paul and Haeberli, 2008), when the SLA is at lower elevation as it was the case in 2001 (2,839±129 m a.s.l.) it is better to use a DEM as close as possible as the date of the used images. Accordingly, the

DEM from the French IGN was used to the first half of the period (till the late 1990s) and the ASTERGDEM was used for the second part of the period. Changing from one DEM to the other in the late 1990s has no impact on the results because at that time, the SLA was located between 3,000 and 3,200 m a.s.l., an altitudinal range for which the difference in elevation between the DEMs is lower than their vertical accuracies.

An uncertainty was estimated for each SLA. Uncertainty results from different sources of error (Rabatel et al., 2002, 2012a): (1) the pixel size of the images, which ranged between 2.5 and 30 m depending on the sensor; (2) the slope of the glacier in the vicinity of the SLA, which ranged from 7° to 32° depending on the glacier and the zone where the SLA was located in any given year; (3) the vertical accuracy of the DEM, which was about 20 m; and (4) the standard deviation of the calculation of the average SLA along its delineation, which ranged from 10 m to 170 m depending on the glacier and on the year concerned. The last source of error (4) is the most important. The resulting total uncertainty of the SLAs (root of the quadratic sum of the different independent errors) ranged from ±15 to ±170 m, depending on the year and glacier concerned. The uncertainty was greater when the SLA was located on a part of a glacier where the slope is steepest because in this case, the standard deviation of the computed SLA is high.

2.2.3. Method used to fill data gaps in the snowline altitude time series

In spite of the large number of images used in this study, there were still some gaps in the SLA time series. In the 27-year study period, for the 43 glaciers studied, the SLA was measured in 85% of the 1,081 cases. Thus, data were missing in 15% of the cases.

To fill these gaps, a bi-linear interpolation was applied. Originally, this approach was used by Lliboutry (1965; 1974) to extract the spatial and temporal terms from a very incomplete table of mass balance measurements (70% gaps) in the ablation zone of Saint Sorlin Glacier. This approach is based on the fact that the glacier mass balance depends on both the site and the time of measurement. This approach was subsequently extended to a set of glaciers in the Alps by Reynaud (1980), and later on, to glaciers in other mountain ranges by Letréguilly and Reynaud (1990). Here, we applied it to our SLA table that had far fewer gaps, writing simply:

188 $$SLA_{it} = \alpha_i + \beta_t + \varepsilon_{it} \quad (1),$$

189 Where SLA_{it} is the snow line altitude of the glacier i for the the year t, α_i is long-term mean for each
190 glacier over the period of record, β_t is a term depending on the year only which is common to all the
191 glaciers analyzed, and , with a table of centered residuals
192 assumed to be independent and Gaussian (N denotes the normal distribution). The purpose is not
193 simply to obtain the α_i and β_t terms, but to estimate each missing value SLA_{it} on glacier i and year t as:

194 $$\hat{\alpha}_i = \frac{1}{T}\sum_{t=1}^{T} SLA_{it} \quad (2),$$

195 $$\hat{\beta}_t = \frac{1}{M}\sum_{i=1}^{M}\left(SLA_{it} - \hat{\alpha}_i\right) \quad (3),$$

196 $$\hat{SLA}_{it} = \hat{\alpha}_i + \hat{\beta}_t \quad (4),$$

197 where T is the number of years of the study period, M is the number of glaciers studied, and the "hat"
198 is a classical statistical estimate.
199 To maximize the consistency of the reconstruction, was calculated using only the years for which
200 no data was missing. However, only six years (out of the 27) had the SLA for each of the 43 glaciers,
201 which is not quite enough to obtain an average SLA that is not too dependant on a specific year.
202 Consequently, the initial dataset was divided into three geographical subsets: the Ecrins Massif, the
203 Vanoise area, and the Mont Blanc Massif, and the computation was applied independently to each one
204 of these subsets. In this way, more years with SLAs for all the glaciers of each subset were available
205 (see Table 3, where the statistics of each subset are presented). The year 1995 was the only exception.
206 For this specific year, because very few values were available, the reconstruction was made
207 considering the three subsets together.
208 The RMSE of ε_{it}, representing the model errors was 73 m. This is less than half the standard deviation
209 of the measured SLAs (174 m), showing that the use of the bi-linear model makes sense on this
210 dataset.

2.3. Meteorological data

Table 1 also lists the weather stations we used, which are located in and around the study area (Figure 1). Among the 105 weather stations available in the Météo-France database (including stations operated by Météo-France and Electricité de France) in the French departments (Hautes-Alpes, Isère, Savoie and Haute-Savoie) in the study area, 40 were selected on the basis of data availability and their proximity to the glacierized areas (except Lyon-Bron weather station which was selected as a regional reference). Among the 40 weather stations, only 20 which had continuous series of winter precipitation and summer temperatures over the period 1984-2010 were finally used. Two weather stations in Switzerland were also used. The climate variables used in the analysis were (1) cumulative positive degree days (CPDD) from May 15 to September 15 for each year *t*, extrapolated to the altitude of 3,000 m a.s.l. using a standard gradient of 6 °C/km (3,000 m a.s.l. being the approximate mean elevation of the SLA of the 43 glaciers studied over the whole study period); and (2) cumulated winter precipitation from September 15 of the year *t-1* to May 15 of the year *t*. During this period, liquid precipitation is negligible at 3,000 m a.s.l.

For the CPDD, the date of September 15 was chosen because it matches the average date of the satellite images used to delineate the snowline. Furthermore, it should be noted that at 3,000 m a.s.l. in our study area, after September 15, CPDD are negligible (Thibert et al., 2013).

2.4. Modeling of the control of the morpho-topographic and climate variables

From our dataset of SLA series, glacier morpho-topographic variables, and climate variables, we propose a simple expansion of Lliboutry's approach (1974) to model and reconstruct the SLA fluctuations of any glacier in our study area over the study period. This approach also enables to quantify the respective control of each morpho-topographic and climate variables on the SLA spatio-temporal variability.

Following the ideas of Eckert et al. (2011), the model is implemented in a hierarchical Bayesian framework (e.g. Wikle, 2003). The main advantage over more empirical approaches is treating the different sources of uncertainty in a consistent manner. For instance, the available information (missing values and repeated observations among correlated glacier series) is "respected" when

238 inferring the spatio-temporal patterns of interest, more specifically: the regression variables relating
239 ELA fluctuations, their morpho-topographic and climate drivers, and their respective weight.
240 In detail, starting from the available SLA table with hollow (i.e. without reconstructed values) and Eq.
241 1, we further decomposed the spatial term as:

242 $$\alpha_i = a_o + \sum_k X_{ki} a_k + V_i \quad (5),$$

243 where a_o is the interannual regional average, X_{ki} are the spatial explanatory variables considered for
244 each glacier, i.e. the morpho-topographic variables: latitude, average altitude, surface area and aspect,
245 and $V_i \sim N\left(0, \sigma_v^2\right)$ is the spatial residual, i.e. the local effect for the glacier *i* which is not explained
246 by the spatial explanatory variables considered.
247 Similarly, the temporal term is decomposed as:

248 $$\beta_t = \sum_k X_{kt} b_k + Z_t \quad (6),$$

249 where the X_{kt} are the temporal explanatory variables considered, i.e. the climate variables summer:
250 CPDD and winter precipitation, and $Z_t \sim N\left(0, \sigma_z^2\right)$ is the temporal residual, i.e. the annual effect
251 common to all glaciers for any year *t* which is not explained by the temporal explanatory variables
252 considered.
253 For the sake of simplicity, the model is fed with reduced standardized variables (by dividing by the
254 standard deviation the difference between each value and the average of the series). This avoids
255 identifiability problems by granting that $\sum_t \beta_t = 0$, and makes the a_k and b_k coefficients more
256 directly interpretable, at least for non heavily correlated explanatory variables (see below).
257 Without the V_i and Z_t terms, the model would be a classical spatio-temporal linear model with easy
258 inference, e.g. with likelihood maximization providing analytical solutions for point estimates and
259 asymptotic standard errors. However, this would not allow us to distinguish between explained and
260 unexplained variance in the spatial and temporal terms. Hence, the V_i and Z_t terms make the model
261 hierarchical, i.e. richer but also more tricky to estimate. This challenge was solved using Bayesian

Markov Chain Monte Carlo methods (MCMC (7), ...s, 1998). As detailed in Eckert et al. (2007; 2010b) for similar problems, the robustness of the inference was checked using tests based on starting different simulation runs at different points of the parameter space (Brooks and Gelman, 1998). Poorly informative *prior* probability distributions were used for all parameters, this standard choice allows to obtain *posterior* estimates only driven by information conveyed by the data. From the joint *posterior* distribution of all parameters, latent variables, and missing values, we retained point estimates (the *posterior* mean), *posterior* standard deviations, and 95% credibility intervals, the Bayesian counterpart of the classical confidence interval (Table 4). The construction of the model ensures that α_i, β_t and ε_{it} are independent. Furthermore V_i and $\sum_k X_{ki} a_k$ are independent, so are Z_t and $\sum_k X_{kt} b_k$. Hence the total variance of the data table is:

$$VAR(SLA_{it}) = VAR\left(\sum_k X_{ki}\, a_k\right) + VAR\left(\sum_k X_{kt} b_k\right) + \sigma_v^2 + \sigma_z^2 + \sigma^2 \quad (7),$$

By analogy to the classical R^2, variance ratios can then be computed to evaluate the respective weight of the different terms in ELA variability:

$$R^2_{topo} = VAR\left(\sum_k X_{ki}\, a_k\right) / VAR(SLA_{it}) \quad (8),$$

$$R^2_{clim} = VAR\left(\sum_k X_{kt}\, b_k\right) / VAR(SLA_{it}) \quad (9),$$

$$R^2_{topo\,res} = \sigma_v^2 / VAR(SLA_{it}) \quad (10),$$

$$R^2_{clim\,res} = \sigma_z^2 / VAR(SLA_{it}) \quad (11),$$

$$R^2_{res} = \sigma^2 / VAR(SLA_{it}) \quad (12).$$

Similarly, ratios can be computed for the spatial and temporal terms solely:

$$R^2_{space} = VAR\left(\sum_k X_{ki} a_k\right) / \left(VAR\left(\sum_k X_{ki} a_k\right) + \sigma_v^2\right) \quad (13),$$

$$R^2_{time} = VAR\left(\sum_k X_{kt} b_k\right) / \left(VAR\left(\sum_k X_{kt} b_k\right) + \sigma_z^2\right) \quad (14),$$

and, getting rid of the random spatio temporal fluctuations, the overall time/space ratio and determination coefficient in the decomposition can be computed as:

$$R^2_{time/space} = \left(VAR\left(\sum_k X_{kt} b_k \right) + \sigma_z^2 \right) / (VAR(SLA_{it}) - \sigma^2) \quad (15),$$

$$R^2_{tot} = \left(VAR\left(\sum_k X_{ki}\, a_k \right) + VAR\left(\sum_k X_{kt} b_k \right) \right) / (VAR(SLA_{it}) - \sigma^2) \quad (16),$$

All these statistics quantify the weight of mean spatial and temporal effects in the total variability, and the capacity of the chosen explanatory variables to model these mean effects. At the observation level of each year/glacier of the model, local and annual adjustment statistics can also be computed as:

$$\delta_t = \frac{-1}{M} \sum_i \varepsilon_{it} \quad (17),$$

$$\delta_i = \frac{-1}{T} \sum_t \varepsilon_{it} \quad (18),$$

$$\delta_t^2 = 1 - \sqrt{\frac{\sum_i \varepsilon_{it}^2}{\sum_i SLA_{it}^2}} \quad (19),$$

$$\delta_i^2 = 1 - \sqrt{\frac{\sum_t \varepsilon_{it}^2}{\sum_t SLA_{it}^2}} \quad (20),$$

respectively the annual and local bias, and the annual and local determination coefficient, with *M* the number of glaciers considered and *T* the number of years studied. They quantify the goodness of fit of each of the annual/local series.

Variance ratios and adjustment statistics were evaluated by computing their values at each point of the MCMC iterative simulation run, giving access to point estimates and related uncertainties taking into account the number of missing values for each year/glacier (logically, when nearly all observations are missing for a given year/glacier, the corresponding determination coefficients δ_t^2 and δ_i^2 are unknown).

3. RESULTS

Here we give the results of both the SLA and the climate variables. In sub-section 3.1., we present the temporal and spatial variability of the SLA measured on the 43 glaciers for the 1984-2010 period. In sub-section 3.2., we present the variability of climate variables (i.e. summer CPDD and winter precipitation).

3.1. Changes in the equilibrium-line altitude

As mentioned above, it has been demonstrated that on mid-latitude glaciers where superimposed ice is negligible, the end-of-summer SLA is an accurate indicator of the ELA (see Figure 6 in Rabatel et al., 2005, and Figure 3B in Rabatel et al., 2008) ~~and is highly correlated with the mass balance in mid-latitude glaciers. Figure 3 illustrates this correlation for three glaciers in the French Alps for which field mass balance measurements are available for the 1984-2010 period.~~ Because of this strong correlation and for the sake of simplicity, we hereafter only use the term ELA.

3.1.1. Temporal variability of the equilibrium-line altitude

Figure 3A illustrates changes in the ELA over the 1984-2010 period for the 43 glaciers studied (see also see supplementary material: Table II where all the data are presented). Considering all the glaciers, the average ELA for the whole period was located at 3,035±120 m a.s.l., i.e. the interannual variability of the average ELA of all glaciers was high (120 m on average). The difference between extreme years was as high as 460 m, with the lowest average ELA measured in 1984 (2,790±180 m a.s.l.), and the highest average ELA measured in 2003 (3,250±135 m a.s.l.). In addition, over the study period, the ELA time series showed an average increasing trend of 6.4 m/yr, assuming a linear trend which results to be statistically significant considering a risk of error of 5%. This is the equivalent of an average increase of 170 m over the 1984-2010 period, i.e. higher than the interannual variability of the average ELA.

The average annual ELA during first five years of the study period was lower than the average ELA for the whole period (except in 1986, when it was slightly higher than average). These years match the end of a 15-year period (from the mid-1970s to the late 1980s) during which alpine glaciers increased in size due to higher winter accumulation and reduced summer ablation (Vincent, 2002; Thibert et al.,

2013). Since 2003, the average annual ELA has consistently been above the average ELA for the whole period. Considering the two subsets, i.e. before and after 2003, no significant trend appeared in either of the subsets. The second subset is shorter (8 years) than the first (19 years), and trends computed on short periods should be interpreted with caution. However, the average ELA between the two subsets increased by about 140 m, which is 82% of the total change. Hence, the year 2003 can also be considered as a breakpoint in the time series. It should be noted that the 2003 extreme heat wave resulted in a reduction, or even complete loss on some glaciers, of the firn area, hence introduced a positive feedback on glacier mass balances after 2003, consistent with higher ELAs.

Considering each glacier individually, Figure 4 shows the rate of increase in the ELA over the whole period for each glacier plotted against its aspect. In this study, the aspect of the glacier matched the average aspect of the area of the glacier, where the ELA fluctuated over the whole study period. It is notable that: (1) the increasing trend of the ELA varied between less than 1 m/yr and more than 13 m/yr depending on the glacier; and (2) glaciers facing east displayed a more pronounced increasing trend of the ELA. However, this result should be interpreted with caution because the distribution of the glaciers studied in not homogeneous with respect to the aspect of the majority of glaciers in the French Alps, which are north facing. Furthermore, one of our selection criteria should also be recalled: to measure the ELA for each year, the glaciers had to reach at least 3,250 m a.s.l. (highest average ELA measured in 2003), and south-facing glaciers reaching this elevation are rare and can only be found in the Mont Blanc Massif.

3.1.2. Spatial variability of the equilibrium-line altitude

Figure 5A shows the results of a factor analysis of the ELA time series including all the glaciers and all the years in the study period. The factor analysis being a statistical method allowing to describe the variability, differences or similitudes among observed and correlated variables according to a lower number of factors, i.e. unobserved variables, for instance the space and time. For the ELA time series, the first two factors explained 80% of the common variance with 71% on the first factor. The high percentage of common variance on factor 1 represents the common temporal signal in the interannual variability of the ELAs that is related to climatic forcing. Factor 2 explained 9% of the common variance of the glaciers studied and is related to different spatial patterns. Hence, with respect to the

second factor, two groups can be distinguished corresponding to the northern Alps (Mont Blanc, Vanoise) and the southern Alps (Ecrins), respectively. One glacier in the Vanoise Massif, Gébroulaz Glacier, is closer to the glacier group of the southern Alps. Its geographic location, i.e. nearest to the southern sector among the Vanoise glaciers, could partly explain the position of this glacier in the graph. The distinction between the two groups could be related to a higher elevation of the ELA for the glaciers of the southern sector (Figure 6A) which could be associated with differences in winter accumulation between the southern and northern Alps (see below) and warmer summer temperature in the southern sector which would increase the amount of CPDD and thus the ablation (note that the effect of higher summer temperature on a shift of precipitation from snow to rain is not considered in this study because we do not use summer precipitation in our analysis). Indeed, Figure 6A shows the average ELA over the 1984-2010 period for each glacier plotted as a function of its latitude: a clear decreasing trend is apparent from south to north, with an average ELA located on average 150 m higher for the glaciers in the southern sector.

3.2. Changes in climate conditions

Figure 3B shows the changes in summer CPDD over the 1984-2010 period for the 22 weather stations used. Summer CPDD present an increasing ~~linear~~ trend, averaging 5.3±1.9 CPDD/yr at 3,000 m a.s.l. assuming a linear trend over the period 1984-2010. This trend is statistically significant considering a risk of error of 5%. Such an increase (150±1.9) in the CPDD over the study period is the equivalent of an additional energy supply of 14±6 W/m², which can result in an additional ablation of about 0.5 m w.e. (assuming that all of this energy is used to melt the snow, and so that sublimation is negligible).

The year 2003 had the maximum summer CPDD in the 1984-2010 period, and 2003 is an outlier in the time series. In this particular year, the ELA was about 300 meters higher than the average for the whole period (in fact above many glacierized summits), and is clearly associated with an unusually warm summer (Beniston and Diaz, 2004) that caused intense ablation, because winter precipitation in 2003 was average for the study period.

Temporal variations in the summer CPDD at 3,000 m a.s.l. were highly homogeneous across the study area. Indeed, the factor analysis of these data (Fig. 5B) showed a common variance of 85% on the first axis indicating similar temporal variations between the stations located up to 150 km apart.

Regarding winter precipitation, no significant ~~linear~~ trend was observed over the study period (Fig. 3C). However, one can note that, on average, interannual variability was lower after 2001 (standard deviation divided by 2 after 2001, falling from 140 mm to 62 mm), but it should be kept in mind that the time series after that date is short, and this point thus needs to be confirmed with longer data series. Over the study period, maximum winter precipitation occurred in 2001, and the same value was almost reached in 1995. These two years correspond to low ELAs, but not to the lowest of the whole time series, which occurred in 1984 and 1985, and appears to be associated more with cooler summer temperatures.

Variations in winter precipitation at the different stations over time were not as homogeneous as the summer CPDD, even if the first factor of the factor analysis explained 71% of total variance (Fig. 5C). As was the case for the ELAs, two groups can be distinguished on the second axis explaining 9% of the variance. This factor analysis showed that most of the variance was common to all the weather stations and was due to large scale precipitation patterns, but that local effects also exist. This is particularly true for the weather stations located in the southern part of the study area, which is influenced by a Mediterranean climate in which some winter precipitation is not only due to typical western disturbances, but also to eastern events coming from the Gulf of Genoa such as the one in December 2008 (Eckert et al., 2010a).

4. DISCUSSION

In this section, we first discuss the bivariate relationships between each of the morpho-topographic variables considered and the average ELA of each glacier for the study period. Then, in the second part, we present the bivariate relationships between the ELA interannual variability and each climate variable. Finally, we exploit the expansion of Lliboutry's approach (1974) that explicitely incorporates both climate and morpho-topographic variables to reconstruct annual ELAs.

4.1. The role of morpho-topographic variables

Figure 6 shows the relationship between the average ELA of each glacier computed over the whole study period and the latitude of the glacier (Fig. 6A), the mean altitude of the glacier (Fig. 6B), the glacier surface area (Fig. 6C), and the glacier aspect (Fig. 6D).

We already mentioned the relationship between the ELA and the latitude (Fig. 6A) in section 3.1.2, where we noted that the average ELA of the glaciers located in the southern part of the study area was about 150 m higher in altitude that the ELA of the glaciers located in the northern part of the study area. This meridional effect is consistent with the drier and warmer conditions associated with the Mediterranean climate that prevails in the southern part of the study area.

Figures 6B and 6C show the relationship between the average ELA and the average altitude of the glacier and the glacier surface area respectively. The correlation between the average ELA and the glacier average altitude was positive, meaning that the lower the average altitude of the glacier, the lower the average ELA. Conversely, the correlation between the average ELA and the glacier surface area was negative, meaning that the smaller the glacier, the higher the ELA. To understand these correlations, one has to keep in mind the relationship between the ELA and the accumulation area ratio (AAR). Indeed, the ELA constitutes the lower limit of the accumulation zone, which represents ~2/3 of the total glacier surface area in a steady state glacier. Accordingly, the wider the accumulation zone, the bigger the glacier, the lower its snout, the lower the mean altitude and consequently the lower the ELA of the glacier. Current ELAs can certainly not represent steady state conditions, nevertheless, over a long period of time (almost 30 years in our case), assuming pseudo-stationary conditions over this period, the average surface area of a glacier as well as its average altitude can be deemed to be representative of its average ELA. This is in good agreement with the results presented by Braithwaite and Raper (2010) showing, on the basis of 94 glaciers, that the glacier area-median and mid-range altitudes are accurate proxies of the ELA for a period of time, e.g. several decades.

Figure 6D shows the average ELA of each glacier plotted as a function of the glacier aspect. For this morpho-topographic variable, we distinguished between the different massifs in the study area, because when treated all together, the effects of aspect and latitude tended to cancel each other out. Indeed, the average ELA of a glacier facing north in the Ecrins Massif is almost the same as the average ELA of a glacier facing south in the Mont Blanc Massif. As a result, the meridional effect

433 related to the latitude is stronger than the aspect effect. However, considering each massif separately,
434 and even if our samples are not homogeneous with respect to aspect, glaciers facing north and east
435 have a lower average ELA than glaciers facing south and west, as would be expected for mid-latitude
436 glaciers in the northern hemisphere.

437 ### 4.2. Climatic control of equilibrium-line altitude interannual variability

438 Analysis of the variances and correlations between the ELA of each glacier and the climate variables
439 (summer CPDD and winter precipitation) was conducted for the study period. Considering our 27-year
440 dataset, the correlation coefficient 'r' is statistically significant with a risk of error lower than 1%
441 when $r > 0.49$, or $r < -0.49$, and lower than 5 % when $r > 0.38$ or $r < -0.38$.
442 Figure 7 shows the correlation coefficients for the two climate variables obtained by selecting the
443 weather station with the highest value for each glacier. The correlation coefficients were plotted
444 against the latitude of the glaciers in order to evaluate spatial variations in these coefficients. For
445 summer CPDD, Figure 7A shows: (1) a generally high and always significant correlation coefficient
446 regardless of the glacier and its location in the study region; (2) a slight but not statistically significant
447 decrease in the correlation coefficient with increasing latitude. This means that the proportion of
448 variance of the ELAs explained by the summer CPDD is, first, important, and secondly, of the same
449 order regardless of the glacier concerned.
450 This also appears clearly in Figure 3 which shows strong similarities between annual variability of
451 ELAs (Fig. 3A) and CPDD (Fig. 3B), mostly an increasing trend over the whole study period,
452 although stronger before 1990, which apparently stopped after the 2003 maximum. Hence, the annual
453 means of both variables are strongly correlated ($r = 0.73$). To further highlight their similarities, a
454 spline regression was performed, which fit the data variability well, apart from the exceptional CPDD
455 in 2003. The correlation between these low frequency signals was enhanced with regards to annual
456 means, reaching $r = 0.84$, confirming the very similar long-term variations in ELA and CPDD over the
457 study area.
458 Regarding winter precipitation, Figure 7B shows the particular behavior of the Ecrins Massif (blue
459 triangles in Fig. 7B), which could be related to a winter precipitation regime influenced by the eastern

460 disturbances coming from the Gulf of Genoa and presenting higher temporal variability than the
461 typical regime in which disturbances come from the west. However, except for three glaciers in the
462 Ecrins Massif, the correlation between the ELA and cumulative winter precipitation was statistically
463 significant considering a risk of error lower than 5%, and even 1% in most cases. These three glaciers
464 are Glacier des Violettes (# 40), Glacier de la Girose (#33) and Glacier du Mont de Lans (#35); the
465 low correlation with precipitation for these glaciers could be due to topographic effects influencing
466 redistribution of the snow by the wind which can affect accumulation processes in one way or the
467 opposite, i.e. over-accumulation or erosion (Girose and Mont de Lans are located on a dome and
468 Violettes in a narrow and cashed mountainside).
469 Hence, the annual average ELAs (Fig. 3A) and winter precipitation (Fig. 3C) were rather strongly
470 negatively correlated (r = -0.63). Like for CPDDs, a well supported spline regression enhanced their
471 similarities (r = -0.80). This showed that the irregularities in the increasing trend of the average ELA
472 at the scale of the study region were linked to winter precipitation anomalies: excesses in 1995 and
473 2001, and deficits in 1990 and 1998, which respectively decreased/increased the annual average ELA.
474 Finally concerning Figure 7, one has to keep in mind that: (1) the highest correlation coefficient was
475 found for summer CPDD; and (2) except for few glaciers in the Ecrins Massif, significant correlations
476 were also found with winter precipitation but to a lesser extent than with summer CPDD. These points
477 are in good agreement with results found at a glacier scale based on direct field measurements
478 showing that the mass balance variability (and hence the ELA) is primarily controlled by summer
479 ablation variability which is in turn closely linked with summer CPDD (e.g. Martin, 1974, Vallon et
480 al., 1998; Vincent, 2002). However, if Figure 3 confirms that the observed increasing trend in the
481 average regional ELA is in fact mainly driven by increasingly warm summer temperatures, it also
482 shows that nonlinear low frequency fluctuations in the average regional ELA are significantly related
483 to winter precipitation anomalies.
484 In terms of sensitivity of the ELA to climate variables, Figure 8 shows the scatter plots of ELA
485 anomalies vs. summer CPDD anomalies (Fig. 8A) and winter precipitation anomalies (Fig. 8B). For
486 this figure, both the ELA anomalies and the summer CPDD and winter precipitation anomalies were
487 computed from the annual average values of the 43 glaciers and the six weather stations with the

488 highest correlation coefficients. These two graphs show that the sensitivity of the ELA to summer
489 temperature was 115 m°C^{-1} (note that the length of the period used to compute the summer CPDD was
490 120 days in our case, and that the temperature gradient used to compute the CPDD at 3,000 m a.s.l.
491 was 6 °CKm^{-1}); and the sensitivity of the ELA to winter precipitation was 48 m/100 mm. This means
492 that an additionnal amount of winter precipitation of about 240 mm is needed to compensate for a
493 daily average increase in summer temperature of 1 °C. Note that in our estimate, we do not consider
494 that the increase in summer temperature would lead to a lengthening of the ablation period.
495 Our estimate of ELA sensitivity to summer temperature, 115 m°C^{-1}, is in the middle range of values
496 reported in the literature which range from 60-70 m°C^{-1} (Vincent, 2002) to 160 m°C^{-1} (Gerbaux et al.,
497 2005). Other values from the European Alps and other mid-latitude, temperate regions that can be
498 found in the literature are: 90-115 m°C-1 (Braithwaite and Zhang, 2000), 100 m°C^{-1} (Zemp et al.,
499 2007), 125 m°C^{-1} (Kuhn, 1981) or 130 m°C^{-1} (Oerlemans and Hoogendoorn ,1989). Such a difference
500 in values mainly results from the approach used that vary from empirical regressions from ablation
501 stake measurements on a monitored glacier and temperature data from one weather station located
502 close to the glacier, to modeling approaches based on physical processes and providing information on
503 the sensitivity of the ELA to all meteorological variables. Here, our approach is empirical, but relies
504 on large number of glaciers and weather stations and can be considered as relevant at the scale of
505 French alpine glaciers.

506 **4.3. About the efficiency of our modeling approach to reconstruct equilibrium-line**
507 **altitude time series from morpho-topographic and climate variables**

508 Figure 9 and 10 summarize the results of the modeling approach from the symmetric temporal and
509 spatial point of views. Hence, in each figure, A and B subplots illustrate the capacity of our method to
510 model the common pattern of time (respectively the interannual local effect), getting rid of the
511 interannual effect of each glacier (respectively the annual common effect). C and D subplots quantify
512 the goodness of fit at the lower level of each annual/local series in terms of bias and determination
513 coefficient.

From Figures 9 and 10 and Table 4, one can first see that the temporal/spatial decomposition is very good, with a low equal to 0.25. This suggests a very clear distinction between the effects of space and time in the total data variability. Furthermore, the average temporal effect for each year and the interannual spatial effect for each glacier are well captured by the symmetric temporal and spatial regression models, with high determination coefficients in time (R^2_{time} = 0.73) and in space (R^2_{space} = 0.72), leading to a total determination coefficient (R^2_{tot} = 0.73). This confirms the capacity of the chosen explanatory variables to model the average spatial and temporal effects.

This is particularly true for the temporal explanatory variables: with only two climate variables, the regression explains more than 30% of total variance (main term), leading to the predominance of interannual fluctuations with regards to interglacier variability ($R^2_{time/space}$ = 0.56). As a consequence, the average annual ELAs modeled from temporal explanatory variables follow annual fluctuations of the mean ELA (β_t series) very well, and roughly match the spline adjustment presented in Fig. 3A. A Spearman test showed that CPDD and winter precipitations are independent, so that, since all the explanatory variables are standardized anomalies, the regression parameters given in Table 4 are directly the marginal correlation coefficient with the β_t series, 0.42 and -0.31, respectively.

For the spatial term, the four morpho-topographic variables explain about R^2_{topo} = 25% of total variance, and R^2_{space} = 72% of the variability of the interannual average ELA for each glacier (α_i series). For the spatial explanatory variables, a slight correlation exists between the surface area and the average elevation of the glaciers. However, the values of a_k (Eq. 5) for each covariate remain close to the correlation values of the bivariate regressions (section 4.1.), suggesting that the model is not over-parameterized so that the full inferred multivariate relationship can be interpreted with reasonable confidence.

Figures 9C and 10C (Fig. 9D and 10D) present the annual and local determination coefficients (the annual and local bias). Since the bias is generally close to zero, and the determination coefficient acceptable, this confirms the overall capacity of the model to reproduce the dataset variability, in accordance with the inferred low R^2_{res} = 0.25 value for each year / each glacier. In other words, the

assumption of complete separability of the effects of space and time appears to be correct for most of the years / glaciers whose ELA time series can be reasonably approximed by the regional annual mean series / interannual local mean series, weighted by the interannual mean effect for each glacier / the regional annual effect for each year, respectively. However, for some years or glaciers, the high bias/low determination coefficients show that this is not true, i.e. that the spatio-temporal decomposition is insufficient to fully represent the variability of ELA values measured using the remote sensing images. For these peculiar years or glaciers, certain points are worth emphasizing to explain the non-negligible spatio-temporal residuals:

- In Figure 9C, the years 1990 and 2008 showed low determination coefficients. This means that for these two years, the ELA variability between the glaciers concerned differed from that of the whole period. Indeed, we mentioned in section 4.1. that, over the whole study period, the average ELA of the glaciers of the southern sector of the study region was about 150 m higher in altitude than that of the glaciers located in the northern sector. In the years 1990 and 2008, the situation was not the same, the ELA was homogeneous in 2008, and, in 1990, the ELA of the glaciers located in the southern sector was lower than the ELA of the ones in the northern sector. This situation is not clearly explained by the climate variables and further investigations are needed to explain what happened during these two years.
- In Figure 9D, the only year with an annual bias higher than ±5 m was the year 2002. It should be noted that the year 2002 followed a year with a very high winter accumulation leading to a low ELA. During the field campains at the end of summer 2002, a firn line (firn from the year 2001) and the snowline were observed. However, the difference between the firn line and the snowline is difficult to distinguish on images with 30 m resolution (most of the ELA in 2002 were measured on Landsat images). As a consequence, it is quite possible that for some of the glaciers studied, the firn line was delineated instead of the snowline. This used to be the limitation of the use of satellite images, however, with the new sensors launched in the recent years that have a resolution of few meters or even tens of centimeters, this limitation is now reduced.
- In Figure 10C, some glaciers (e.g. Gébroulaz or Violettes glaciers) show low determination coefficient. This means that for these glaciers, the ELA interannual variability differed from the

568 one computed for all the glaciers studied. For Gébroulaz Glacier, Rabatel et al. (2005) had already
569 reported specific behavior. These authors assumed that the peculiar accumulation conditions on
570 this glacier could lead to a low mass-balance gradient. This could be one of the causes of the
571 different interannual variability of the ELA on this glacier. For Violettes Glaciers (the only
572 glacier with a local bias above 15 m, Fig. 10D), as already mentioned in section 4.2., the peculiar
573 morpho-topographic conditions could be responsible for the different interannual variability of its
574 ELA.
575

5. CONCLUSION

This study presents time series of ELA for 43 glaciers located in the western Alps over the 1984-2010 time period. ELAs were derived from the end-of-summer snowline altitude, an accurate proxy of the ELA for mid-latitude mountain glaciers. More than 120 satellite images were used to obtain an annual coverage of the 43 glaciers during the 27-year period. In parallel, this study analyzed changes in climate variables in terms of summer CPDD and winter precipitation. These two variables were obtained for the same time period from 22 weather stations located in and around the study area. From these time series several points are worth emphasizing:

- Assuming a linear trend over the study period: the average ELA increased by about 170 m; the summer CPDD increased by about 150 PDD at 3,000 m a.s.l. while winter precipitation remained rather stationary.
- Temporal variability of the ELAs, summer CPDD and winter precipitation were very homogeneous over the study region. Regarding spatial variability, homogeneity was high for summer CPDD, but glaciers in the southern part of the study area differed from the others.

Bivariate and relationships between the ELAs and morpho-topographic and climate variables were also establihed. These relationships allow us to highlight the fact that:

- The average ELA over the study period of each glacier is strongly controlled by its morpho-topographic variables, namely its average altitude, surface area, latitude and aspect.
- The interannual variability of the average ELA of the glaciers studied is strongly controlled by climate variables, with the observed increasing trend in the average ELA truly mainly driven by increasingly warm temperatures, even if nonlinear low frequency fluctuations in the average ELA time series appear to be significantly related to winter precipitation anomalies.

From these relationships, we propose an expansion of Lliboutry's approach, implemented within a hierarchical Bayesian framework, to reconstruct the ELA fluctuations of any glacier in the study area. Considering two climate variables and four morpho-topographics variables, we show that our approach is well suited to: (1) isolate an average temporal effect for each year and an interannual mean effect for each glacier; (2) model and explain their fluctuations from a reduced number of climatic and topographic explanatory variables whose respective weight and related uncertainties are quantified in a

consistent manner; and (3) well approximate the full variability of our ELA dataset for each year and for each glacier and identify specific spatio-temporal behaviors that do not match the assumption of complete separability of space and time effects.

Finally, both methods presented in this study, based on remote sensing and modeling, are powerful tools to provide annual series of ELA that will be useful in hydrological modeling of high mountain watersheds where there is a need to integrate the glacier component in such an approach and when no field data are available.

Acknowledgements

This study was conducted in the context of the French glacier observatory GLACIOCLIM (http://www-lgge.ujf-grenoble.fr/ServiceObs/index.htm). We are grateful to Imanol Goni for his help with image processing. This work was possible thanks to the contributions of: Météo-France, Electricité de France and Météo-Suisse who provided the meteorological data, USGS-EDC and GLIMS program who granted free access to Landsat images and ASTER images respectively. SPOT images were provided through the CNES/SPOT-Image ISIS program, contracts # 0103-157, 0412-725, 2010-405 and 2010-435. We thank G. Hilmar Gudmundsson (handling editor), M. Zemp and an anonymous referee for their constructive comments used to improve the paper.

References

Barcaza, G., Aniya, M., Matsumoto, T., and Aoki, T.: Satellite-derived equilibrium lines in Northern Patagonia Icefield, Chile, and their implications to glacier variations, Arct. Antarct. Alp. Res., 41(2), 174-182, doi: 10.1657/1938-4246-41.2.174, 2009.

Baltsavias, E.P., Favey, E., Bauder, A, Bosch, H., and Pateraki, M.: Digital surface modelling by airborne laser scanning and digital photogrammetry for glacier monitoring, Photogramm. Rec., 17, 243-273, doi: 10.1111/0031-868X.00182, 1999.

Beniston, M., and Diaz, H.F.: The 2003 heat wave as an example of summers in a greenhouse climate? Observations and climate model simulations for Basel, Switzerland, Glob. Planet. Change, 44 (1-4): 73-81, doi: 10.1016/j.gloplacha.2004.06.006, 2004.

Berthier, E., Arnaud, Y., Baratoux, D., Vincent, C., and Rémy F.: Recent rapid thinning of the ''Mer de Glace'' glacier derived from satellite optical images, Geophys. Res. Lett., 31, L17401, doi: 10.1029/2004GL020706, 2004.

Braithwaite, R.J.: Can the mass balance of a glacier be estimated from its equilibrium-line altitude? J. Glaciol., 30(106), 364-368, 1984.

Braithwaite, R.J., and Zhang, Y.: Sensitivity of mass balances of five Swiss glaciers to temperature changes assessed by tuning a degreeday model, J. Glaciol., 46(152), 7-14, 2000.

Braithwaite, R.J., and Raper, S.C.B.: Estimating equilibrium-line altitude (ELA) from glacier inventory data, A. Glaciol., 50(53), 127-132, doi: 10.3189/172756410790595930, 2010.

Brooks, S.P.: Markov Chain Monte Carlo method and its application, The Statistician, 47(1), 69-100, doi: 10.1111/1467-9884.00117, 1998.

Brooks, S.P., and Gelman, A.: General methods for monitoring convergence of iterative simulations, J. Comput. Graph. Stat., 7(4), 434-455, 1998.

Clare, G.R., Fitzharris, B., Chinn, T., and Salinger, M.: Interannual variation in end-of-summer snowlines of the Southern Alps of New Zealand, and relationships with southern hemisphere atmospheric circulation and sea surface temperature patterns, Int. J. Climatol., 22, 107-120, doi: 10.1002/joc.722, 2002.

649 Chinn, T., Heydenrych, C., and Salinger, M.: Use of the ELA as a practical method of monitoring
650 glacier response to climate in New Zealand's Southern Alps, J. Glaciol., 51(172), 85-95, doi:
651 10.3189/172756505781829593, 2005.
652 Dedieu, J.-P., and Reynaud, L.: Télédétection appliquée au suivi des glaciers des Alpes françaises »,
653 Houille Blanche (5), 355-358, 1990.
654 Demuth, M.N. and Pietroniro, A.: Inferring glacier mass balance using RADARSAT: results from
655 Peyto Glacier, Canada, Geogr. Ann., 81A(4): 521-540, doi: 10.1111/1468-0459.00081, 1999.
656 Eckert, N., Parent, E., Belanger, L., and Garcia, S.: Hierarchical modelling for spatial analysis of the
657 number of avalanche occurrences at the scale of the township, Cold Reg. Sci. Technol., 50, 97-112,
658 doi: 10.1016/j.coldregions.2007.01.008, 2007.
659 Eckert, N., Coleou, C., Castebrunet, H., Giraud, G., Deschatres, M., and Gaume, J.: Cross-comparison
660 of meteorological and avalanche data for characterising avalanche cycles: the example of December
661 2008 in the eastern part of the French Alps, Cold Reg. Sci. Technol., 64(2) 119-136, doi:
662 10.1016/j.coldregions.2010.08.009, 2010a.
663 Eckert, N., Naaim, M., and Parent, E.: Long-term avalanche hazard assessment with a Bayesian depth-
664 averaged propagation model, J. Glaciol., 56(198), 563-586, doi: 10.3189/002214310793146331,
665 2010b.
666 Eckert, N., Baya, H., Thibert, E., and Vincent, C.: Extracting the temporal signal from a winter and
667 summer mass-balance series: application to a six-decade record at Glacier de Sarennes, French Alps,
668 J. Glaciol., 57(201), 134-150, doi: 10.3189/002214311795306673, 2011.
669 Echelmeyer, K., Harrison, W., Larsen C., Sapiano, J., Mitchell, J.E., Demallie, J., Rabus, B.,
670 Adalgeirsdottir, G., and Sombardier, L.: Airborne surface profiling of glaciers: A case-study in
671 Alaska, J. Glaciol., 42, 538-547, 1996.
672 Gardelle, J., Berthier, E., and Arnaud, Y.: Impact of resolution and radar penetration on glacier
673 elevation changes computed from DEM differencing, J. Glaciol., 58(208), 419-422, doi:
674 10.3189/2012JoG11J175, 2012.

675 Gerbaux, M., Genthon, C., Etchevers, P., Vincent, C., and Dedieu, J.-P.: Surface mass balance of
676 glaciers in the French Alps: distributed modelling and sensitivity to climate change, J. Glaciol.,
677 51(175), 561-572, doi: 10.3189/172756505781829133, 2005.
678 Kuhn, M.: Climate and glaciers, IAHS, 131, 3–20, 1981.
679 Lavigne, A., Bel, L., Parent, E., and Eckert, N.: A model for spatio-temporal clustering using
680 multinomial probit regression: application to avalanche counts in the French Alps, Envirometrics,
681 23, 522–534, 2012.
682 Letréguilly, A. and Reynaud, L.: Space and time distribution of glacier mass-balance in northern
683 hemisphere, Arct. Alp. Res., 22(1), 43-50, 1990.
684 Lliboutry, L.: Traité de glaciologie. Tome II: Glaciers, variations du climat, sols gelés. Paris, Masson
685 et Cie., 1965.
686 Lliboutry, L.: Multivariate statistical analysis of glacier annual balances, J. Glaciol., 13(69), 371-392,
687 1974.
688 Machguth, H., Paul, F., Kotlarski, S., and Hoelzle, M.: Calculating distributed glacier mass balance
689 for the Swiss Alps from regional climate model output: A methodical description and interpretation
690 of the results, J. Geophys. Res., 114, D19106, doi: 10.1029/2009JD011775, 2009.
691 Mathieu, R., Chinn, T., and Fitzharris, B.: Detecting the equilibrium-line altitudes of New Zealand
692 glaciers using ASTER satellite images, N.Z. J. Geol. Geophy., 52(3), 209-222, doi:
693 10.1080/00288300909509887, 2009.
694 Martin, S.: Corrélation bilans de masse annuels-facteurs météorologiques dans les Grandes Rousses,
695 Z. Gletscherk. Glazialgeol., BD. X, S. 89-100, 1974.
696 Marzeion, B., Hofer, M., Jarosch, A.H., Kaser, G., and Mölg, T.: A minimal model for reconstructing
697 interannual mass balance variability of glaciers in the European Alps, Cryosphere, 6, 71-84, doi:
698 10.5194/tc-6-71-2012, 2012.
699 Meier, M.F.: Remote sensing of snow and ice, Hydrol. Sci. Bul., 25(3) 9, 307-330, 1980.
700 Oerlemans, J. and Hoogendoorn, N. C.: Mass-balance gradients and climate change, J. Glaciol., 35,
701 399-405, 1989.

Østrem, G.: ERTS data in glaciology – an effort to monitor glacier mass balance from satellite imagery, J. Glaciol., 15(73), 403-415, 1975.

Paul, F., and Haeberli, W.: Spatial variability of glacier elevation changes in the Swiss Alps obtained from two digital elevation models, Geophys. Res. Lett., 35, L21502, doi:10.1029/ 2008GL034718, 2008.

Rabatel, A., Dedieu, J.-P., and Reynaud, L.: Reconstitution des fluctuations du bilan de masse du Glacier Blanc (Massif des Ecrins, France) par télédétection optique (imagerie Spot et Landsat), Houille Blanche (6/7), 64-71, 2002.

Rabatel, A., Dedieu, J.-P., and Vincent, C.: Using remote-sensing data to determine equilibrium-line altitude and mass-balance time series: validation on three French glaciers, 1994-2002, J. Glaciol., 51(175), 539-546, doi: 10.3189/172756505781829106, 2005.

Rabatel, A., Dedieu, J.-P., Thibert, E., Letreguilly, A., and Vincent, C.: 25 years (1981-2005) of equilibrium-line altitude and mass-balance reconstruction on Glacier Blanc, French Alps, using remote-sensing methods and meteorological data, J. Glaciol., 54(185), 307-314, doi: 10.3189/002214308784886063, 2008.

Rabatel, A., Bermejo, A., Loarte, E., Soruco, A., Gomez, J., Leonardini, G., Vincent, C., and Sicart, J.E.: Relationship between snowline altitude, equilibrium-line altitude and mass balance on outer tropical glaciers: Glaciar Zongo - Bolivia, 16°S and Glaciar Artesonraju - Peru, 9°S, J. Glaciol., 58(212), 1027-1036, doi: 10.3189/2012JoG12J027, 2012a.

Rabatel, A., Dedieu, J.-P., Letréguilly, A., and Six, D.: Remote-sesing monitoring of the evolution of glacier surface area and equilibrium-line altitude in the French Alps, Proceedings of the 25th symposium of the International Association of Climatology, 5-8 September 2012, Grenoble, France, 2012b.

Rees, W.G.: Remote sensing of snow and ice. CRC Press, Boca Raton, Florida, 285 p., 2005.

Reynaud, L.: Can the linear balance model be extended to the whole Alps? IAHS AISH, 126, 273-284, 1980.

728 Thibert, E., Eckert, N., and Vincent, C.: Climatic drivers of seasonal glacier mass balances: an
729 analysis of 6 decades at Glacier de Sarennes (French Alps), Cryosphere, 7, 47-66, doi: 10.5194/tc-7-
730 47-2013, 2013.
731 Vallon, M., Vincent, C., and Reynaud, L.: Altitudinal gradient of mass balance sensitivity to climatic
732 change from 18 years of observations on glacier d'Argentiere, France, J. Glaciol., 44, 93-96, 1998.
733 Vincent, C.: Influence of climate change over the 20th Century on four French glacier mass balances,
734 J. Geophys. Res., 107(D19), 4375, doi: 10.1029/2001JD000832, 2002.
735 Wikle, C.: Hierarchical Bayesian models for predicting the spread of ecological processes, Ecology,
736 84(6), 1382-1394, doi: 10.1890/0012-9658, 2003.
737 WGMS: Fluctuations of Glaciers 2005–2010, Volume X, edited by: Zemp, M., Frey, H., Gärtner-
738 Roer, I., Nussbaumer, S.U., Hoelzle, M., Paul, F., and Haeberli, W.,
739 ICSU(WDS)/IUGG(IACS)/UNEP/UNESCO/WMO, World Glacier Monitoring Service, Zurich,
740 Switzerland, 336 pp., publication based on database version: doi:10.5904/wgms-fog-2012-11, 2012.
741 Zemp, M., Hoelzle, M., and Haeberli, W.: Distributed modelling of the regional climatic equilibrium
742 line altitude of glaciers in the European Alps, Glob. Planet. Change, 56, 83-100, doi:
743 10.1016/j.gloplacha.2006.07.002, 2007.
744

745 **Table 1:** List of the glaciers studied and the weather stations used in this study. Numbers (for the
746 glaciers) and codes (for the weather stations) refer to Figure 1. All glaciers are located in the French
747 Alps except when specified in brackets: CH = Switzerland and IT = Italy. For the weather stations,
748 letters in brackets identify the data producer: MF = Météo-France, EDF = Electricité de France, MS =
749 Météo-Suisse. The coordinates are given in degrees, minutes, for latitude and longitude and in m a.s.l.
750 for elevation.

Glaciers				Weather stations	
#	Name	#	Name	Name (data producer) – Code on Fig. 1	Coord.
1	Trient (CH)	23	Grand Méan	Chamonix-Mt-Blanc (MF) – Cham.	45°55' N; 06°52' E; 1042
2	Tour	24	Pelve	Contamine-sur-Arve (MF) – *Off the map*	46°07' N; 06°20' E; 452
3	Saleina (CH)	25	Vallonnet	Contamines-Montjoie (EDF) – Cont.M	45°49' N; 06°43' E; 1180
4	Argentière	26	Arpont	Hauteluce (EDF) – Haut	45°46' N; 06°38' E; 1215
5	Talèfre	27	Mahure	Bourg-Saint-Maurice (MF) – Bg.StM	45°36' N; 06°45' E; 865
6	Pré de Bar (IT)	28	Gébroulaz	Peisey-Nancroix (EDF) – Pe.Na	45°32' N; 06°45' E; 1350
7	Triolet (IT)	29	Baounet	Pralognan-La-Vanoise (EDF) – Pra.laV	45°23' N; 06°43' E; 1420
8	Leschaux	30	Rochemelon	Bessans (EDF) – Bes	45°19' N; 06°59' E; 1715
9	Mont Blanc (IT)	31	Saint Sorlin	Termignon (MF) – Ter	45°16' N; 06°48' E; 1280
10	Freiney (IT)	32	Quirlies	Lyon – Bron (MF) – *Off the map*	45°43' N; 04°56' E; 198
11	Brouillard (IT)	33	Girose	St-Etienne-de-St-Geoirs (MF) – *Off the map*	45°21' N; 05°18' E; 384
12	Tré la Tête	34	Lautaret	Allemond (EDF) – *Off the map*	45°12' N; 06°02' E; 1270
13	Lée Blanche (IT)	35	Mont de Lans	Vaujany (EDF) – Vau	45°09' N; 06°02' E; 772
14	des Glaciers	36	Selle	Besse-en-Oisans (EDF) – B. en O	45°04' N; 06°10' E; 1525
15	Rutor (IT)	37	Casset	La Grave (EDF) – LaG	45°03' N; 06°17' E; 1780
16	Savinaz	38	Blanc	Monetier-Les-Bains (EDF) – M.lesB	44°58' N; 06°30' E; 1459
17	Gurraz	39	Vallon Pilatte	St-Christophe-en-Oisans (EDF) – StC	44°56' N; 06°11' E; 1570
18	Sassière	40	Violettes	Pelvoux (EDF) – Pel	44°52' N; 06°28' E; 1260
19	Tsantelaina (IT)	41	Rouies	Chapelle-en-Valgaudemar (EDF) – *Off the map*	44°48' N; 06°11' E; 1270
20	Grande Motte	42	Sélé	Embrun (MF) – *Off the map*	44°33' N; 06°30' E; 871
21	Mulinet	43	Pilatte	Genève (MS) – *Off the map*	46°14' N; 06°05' E; 420
22	Arcellin			Grand St Bernard (MS) – *Off the map*	45°52' N; 07°10' E; 2472

751

752 **Table 2:** Characteristics of the wavelength of the spectral bands used to identify the snowline on the
753 satellite images of the three sensors.

	Wavelength (µm)		
	Green	**Near-infrared**	**Short-wave infrared**
Landsat	0.52 - 0.60	0.77 - 0.90	1.55 - 1.75
SPOT	0.50 - 0.59	0.79 - 0.89	1.60 - 1.70
ASTER	0.52 - 0.60	0.76 - 0.86	1.58 - 1.75

754

755 **Table 3:** Statistics of the three subsets used to reconstruct missing values.

Name of subset	Number of glaciers	Missing values	Number of complete years used for α_i	RMSE SLA	RMSE ε_{it}
Ecrins	13	11%	14	148 m	62 m
Vanoise	16	20%	12	160 m	66 m
Mont Blanc	14	14%	14	201 m	90 m

756

757 **Table 4:** Posterior characteristics of the proposed model applied on the 43 ELA time series for the
758 1984-2010 period. a_k and b_k denote the regression parameters for each covariate in brackets. 2.5% and
759 97.5% denote the lower and upper bound of the 95% credible interval.

	Mean	**2.5%**	**97.5%**
a_1 (average altitude)	0.381	0.257	0.502
a_2 (latitude)	-0.123	-0.269	0.023
a_3 (aspect)	0.108	-0.022	0.238
a_4 (surface area)	-0.066	-0.199	0.067
b_1 (summer CPDD)	0.417	0.268	0.557
b_2 (winter precipitation)	-0.311	-0.459	-0.155
R^2_{clim}	0.31	0.19	0.41
$R^2_{clim\ res}$	0.11	0.06	0.19
R^2_{topo}	0.24	0.16	0.32
$R^2_{topo\ res}$	0.09	0.05	0.14
R^2_{res}	0.25	0.19	0.30
R^2_{tot}	0.73	0.60	0.81
R^2_{space}	0.72	0.57	0.82
R^2_{time}	0.73	0.52	0.84
$R^2_{time/space}$	0.56	0.43	0.68

760

761 **Figure 1:** The 43 glaciers studied (red) among the 593 glaciers in the French alpine glacier inventory
762 (in blue) plus additionnal glaciers on the Italian and Swiss sides of the Franco-Italian and Franco-
763 Swiss borders. The three boxes represent the main glacierized ranges quoted in the text and figures,
764 i.e. Mont Blanc, Vanoise and Ecrins.

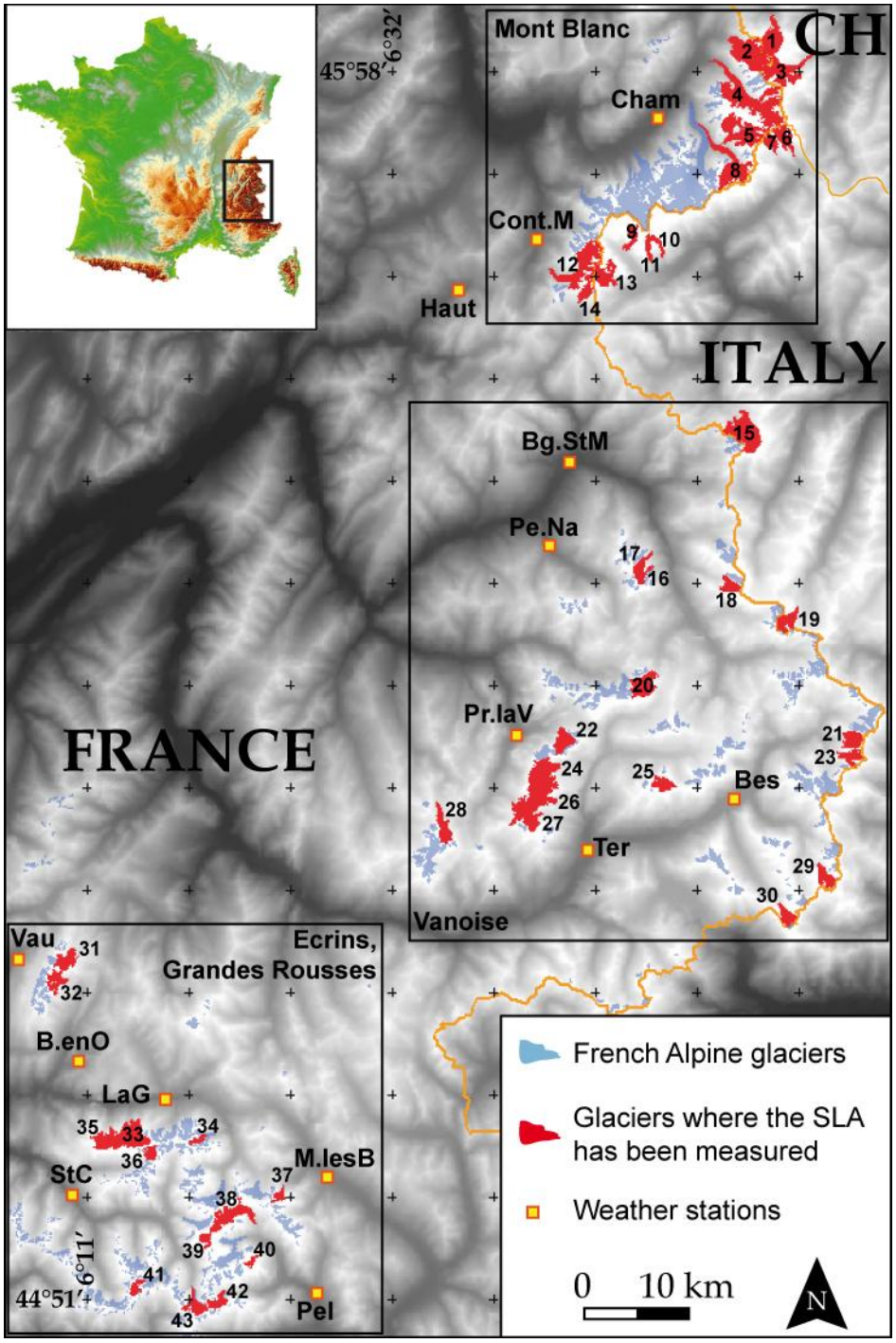

765

766

767 **Figure 2:** Example of Landsat image used to delineate the snowline (red line) with a combination of
768 spectral bands: green, near-infrared and short-wave infrared. Argentière Glacier (Mont Blanc Massif),
769 Landsat TM5 image acquired on September 9, 1987.

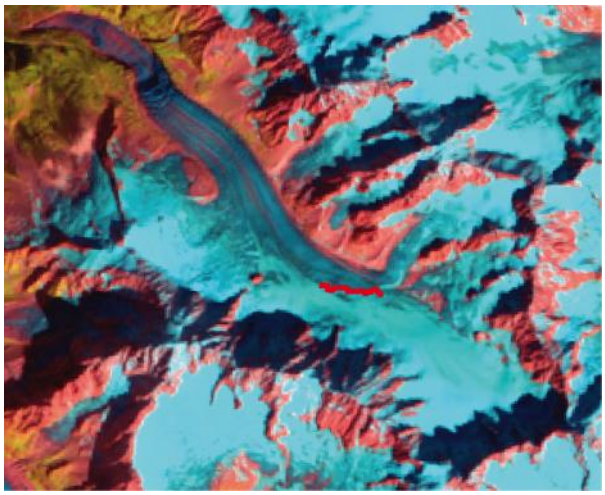

770

771

Figure 3: Changes over the 1984-2010 period in **A)** the ELA for the 43 glaciers studied (see Fig. 1 and Table 1); **B)** summer CPDD; and **C)** winter precipitation recorded by the weather stations used (see Fig. 1 and Table 1). In each graph, the horizontal black bar represents the annual average of the sample, the gray box represents the median interval (Q3-Q1), and the vertical black lines show the interval between the first and the last decile (D1 and D9). On each graph (described in sections 3.1.1. and 3.2.), the dashed line represents the smooth underlying trend captured by a cubic smoothing spline regression (Lavigne et al., 2012). The dotted line is the corresponding 95% credible interval. The yellow and purple boxes highlight the years in which the average ELA at the scale of the study region is linked with positive (yellow) or negative (purple) winter precipitation anomalies (see section 4.2).

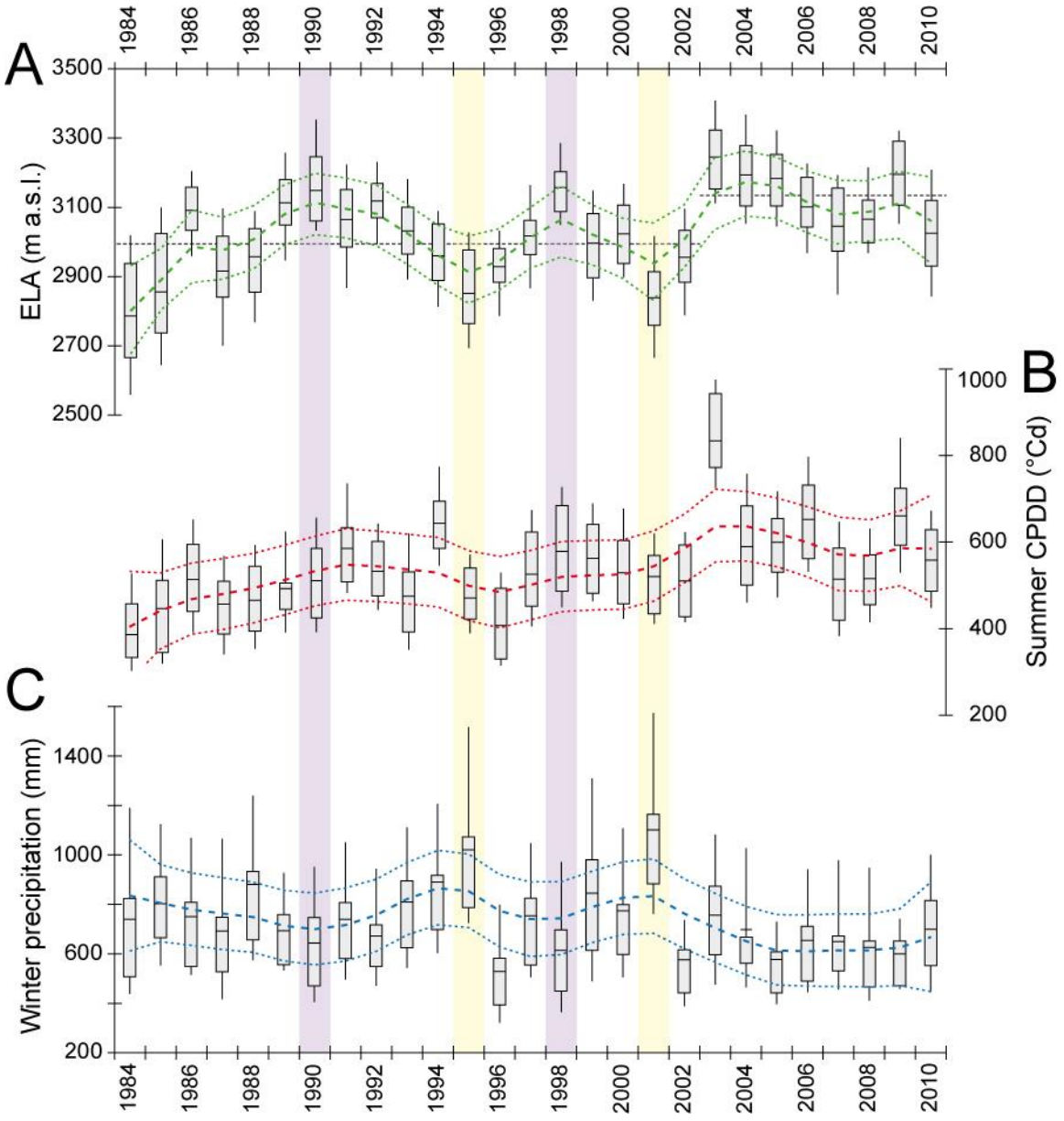

783 **Figure 4:** Average increasing rate of the ELA (m/year) over the 1984-2010 period of each of the
784 glaciers studied with respect to the aspect of the glacier. The color of the diamond identifies the massif
785 in which the glacier is located: blue = Ecrins, green = Vanoise, red = Mont Blanc.

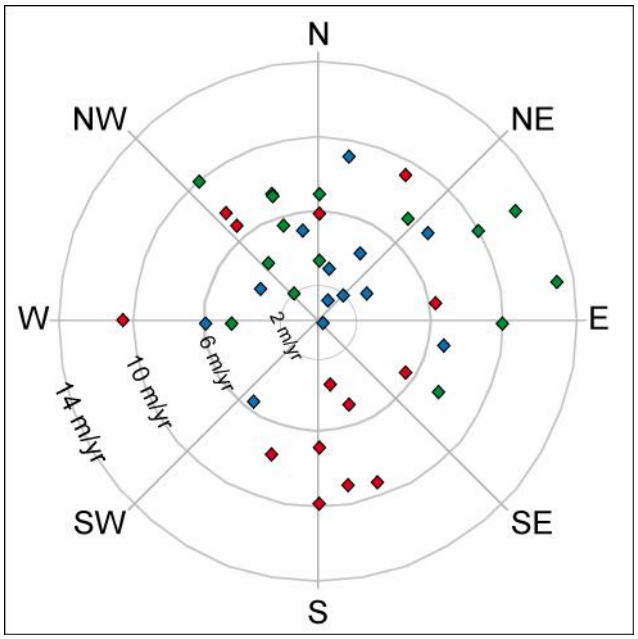

786

787

788 **Figure 5:** Factor analysis of A) the ELAs measured on satellite images; B) the summer CPDD
789 computed from weather stations; and C) winter precipitation computed from weather stations. Detailed
790 information about each graph is provided in the text.

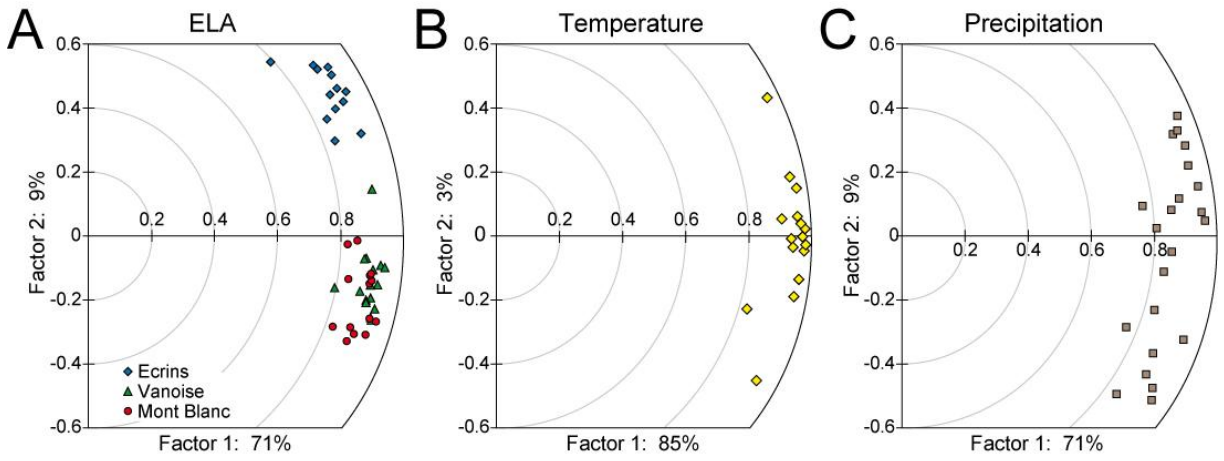

791

792

Figure 6: Average ELA of each one of the 43 glaciers studied over the 1984-2010 period as a function of **A)** glacier latitude, **B)** glacier mean altitude, **C)** glacier surface area, and **D)** glacier aspect. The color of the diamonds in A and D identifies the massif in which the glacier is located: blue = Ecrins, green = Vanoise, red = Mont Blanc.

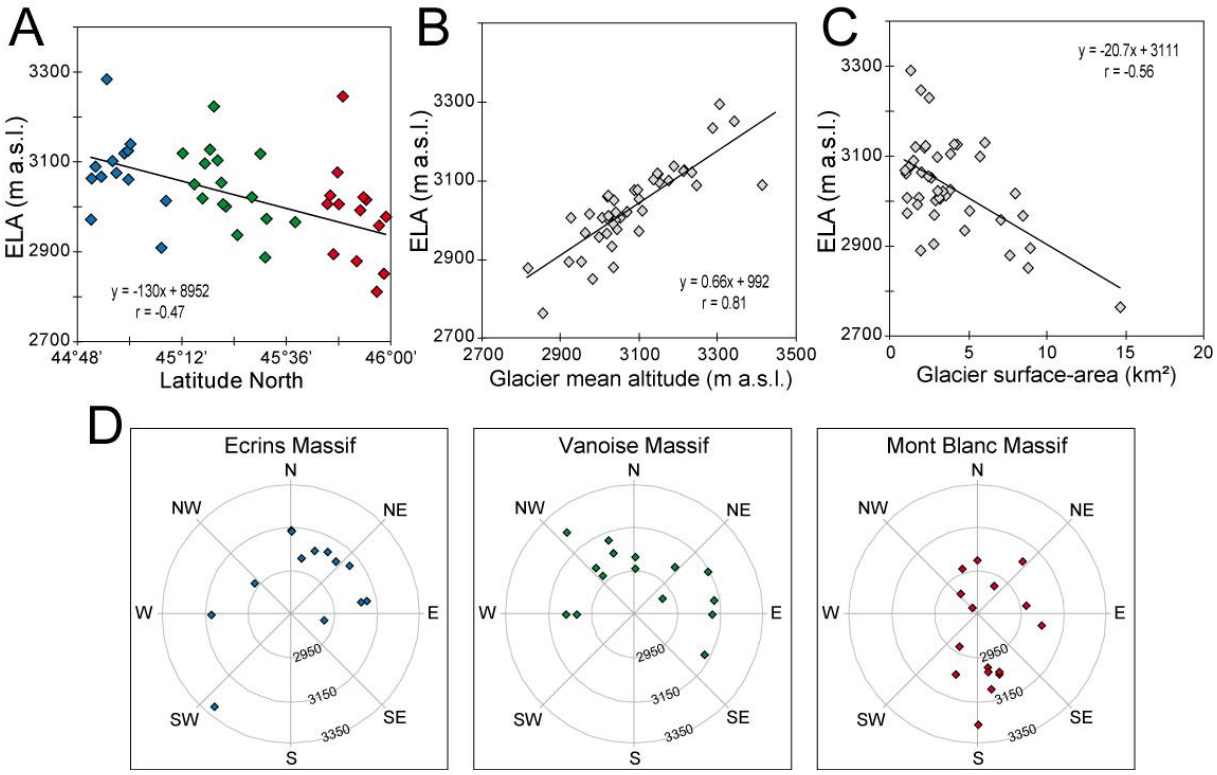

799 **Figure 7: A)** Highest correlations among all the possible 'glacier vs. station' pairs between each
800 glacier (each symbol represents one glacier) and CPDD, plotted as a function of latitude. **B)** The same
801 but with the winter precipitation.

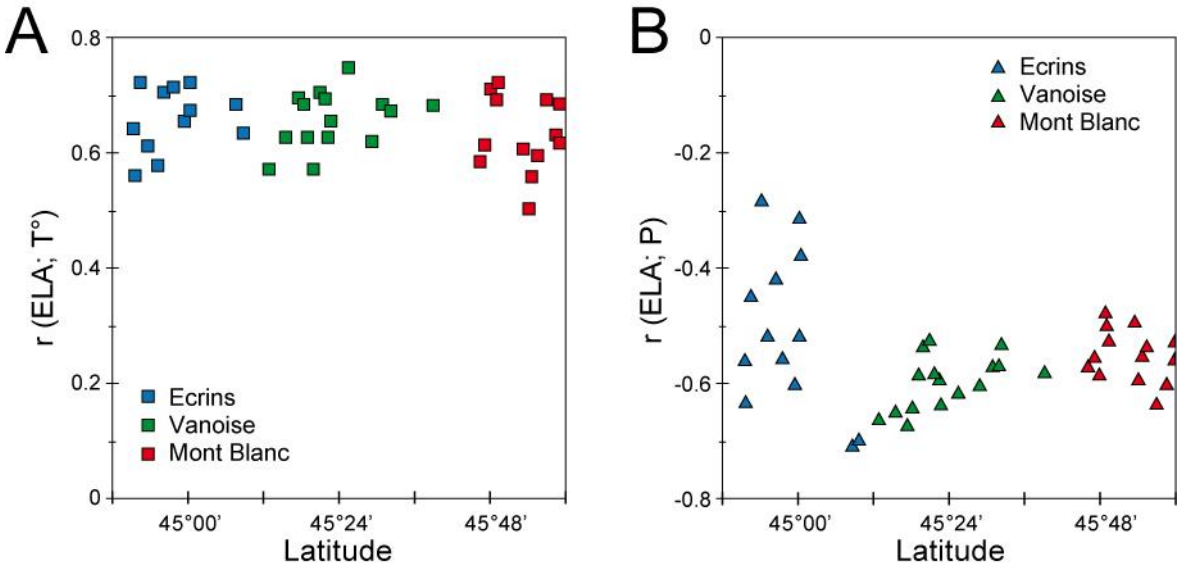

802

803

804 **Figure 8:** ELA anomalies (in meters) plotted versus CPDD anomalies (in °Cd, left graph) and
805 precipitation anomalies (in mm, right graph). Each symbol reprensents one year in the 1984-2010
806 period.

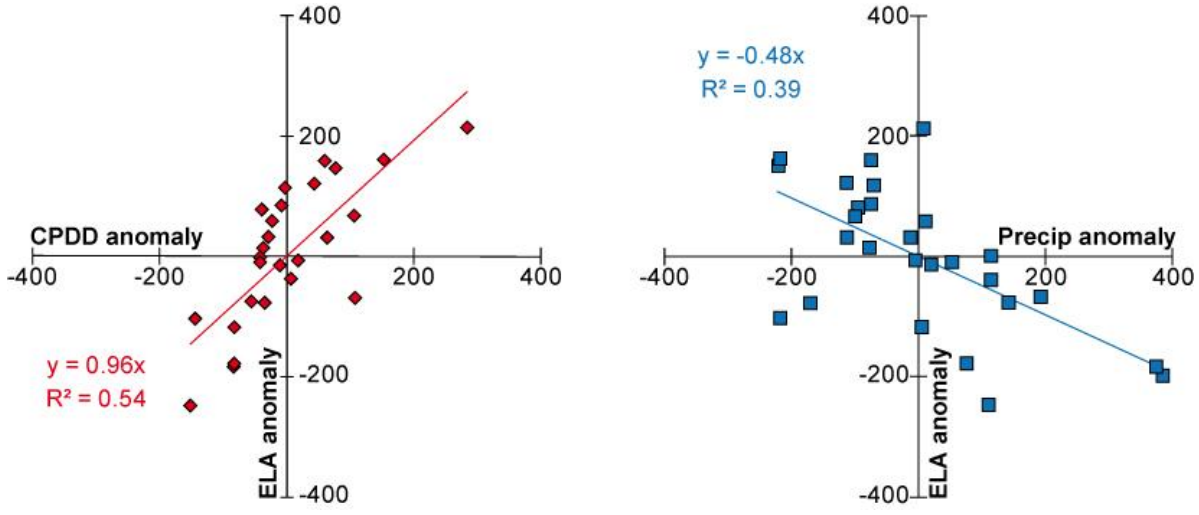

807

808

Figure 9: Results of temporal modeling. **A)** and **B)** show the comparison between the ELA measured on the satellite images and the annual average ELA modeled using the temporal explanatory variables only, thus getting rid of the interannual mean specificity of each glacier. $a_o + \beta_t$ (Eq. 6) is the same plus "white noise" not explained by the temporal explanatory variables. **C)** and **D)** quantify the goodness of the fit for each annual series in terms of determination coefficient and bias, respectively.

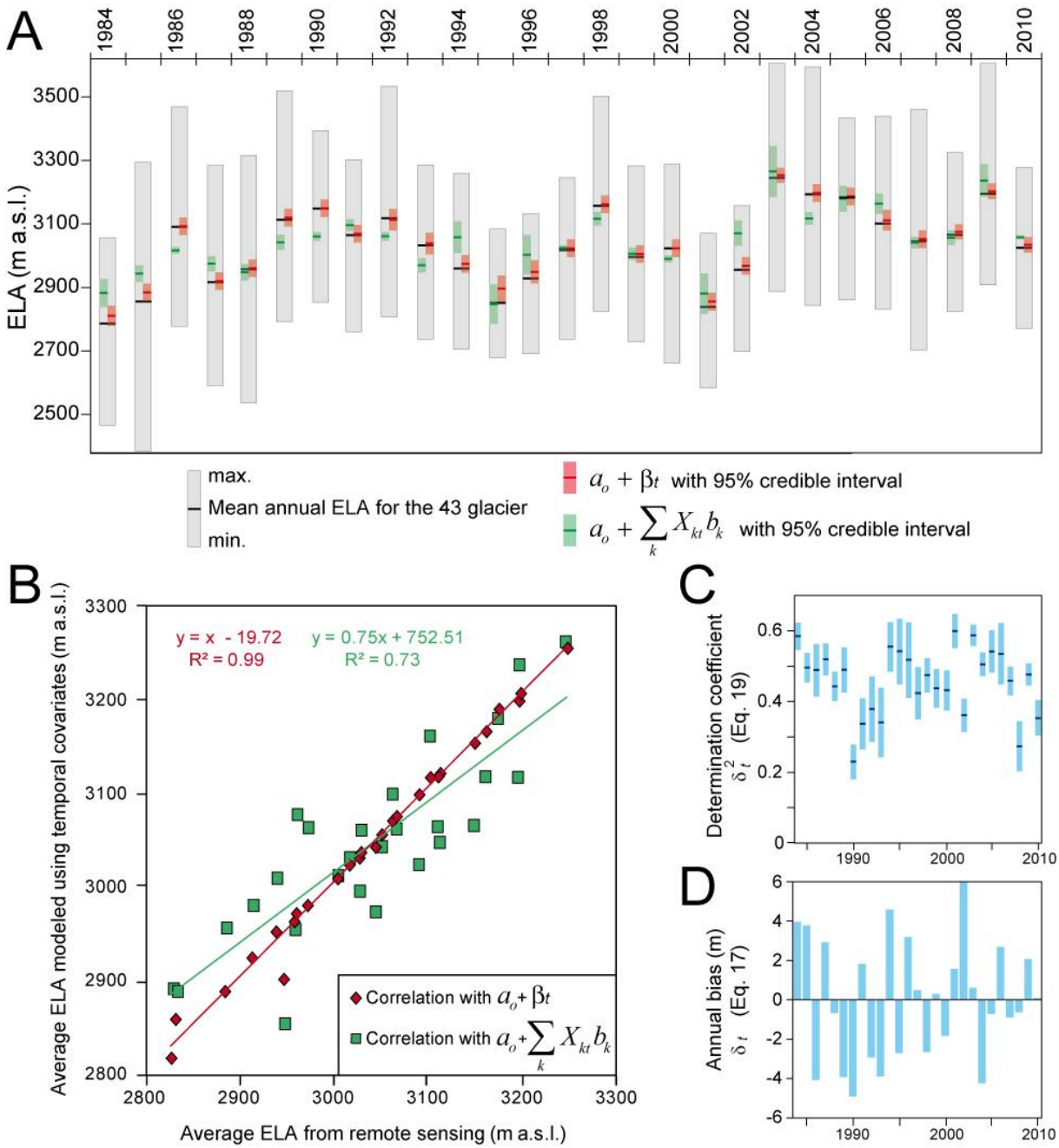

Figure 10: Results of spatial modeling. **A)** and **B)** show the comparison between the ELA measured on the satellite images and the average ELA modeled using the spatial explanatory variables only, thus getting rid of the annual effect common to all glaciers. α_i (Eq. 5) is the same plus "white noise" not explained by the spatial explanatory variables. **C)** and **D)** quantify the goodness of fit for each local series in terms of determination coefficient and bias, respectively.

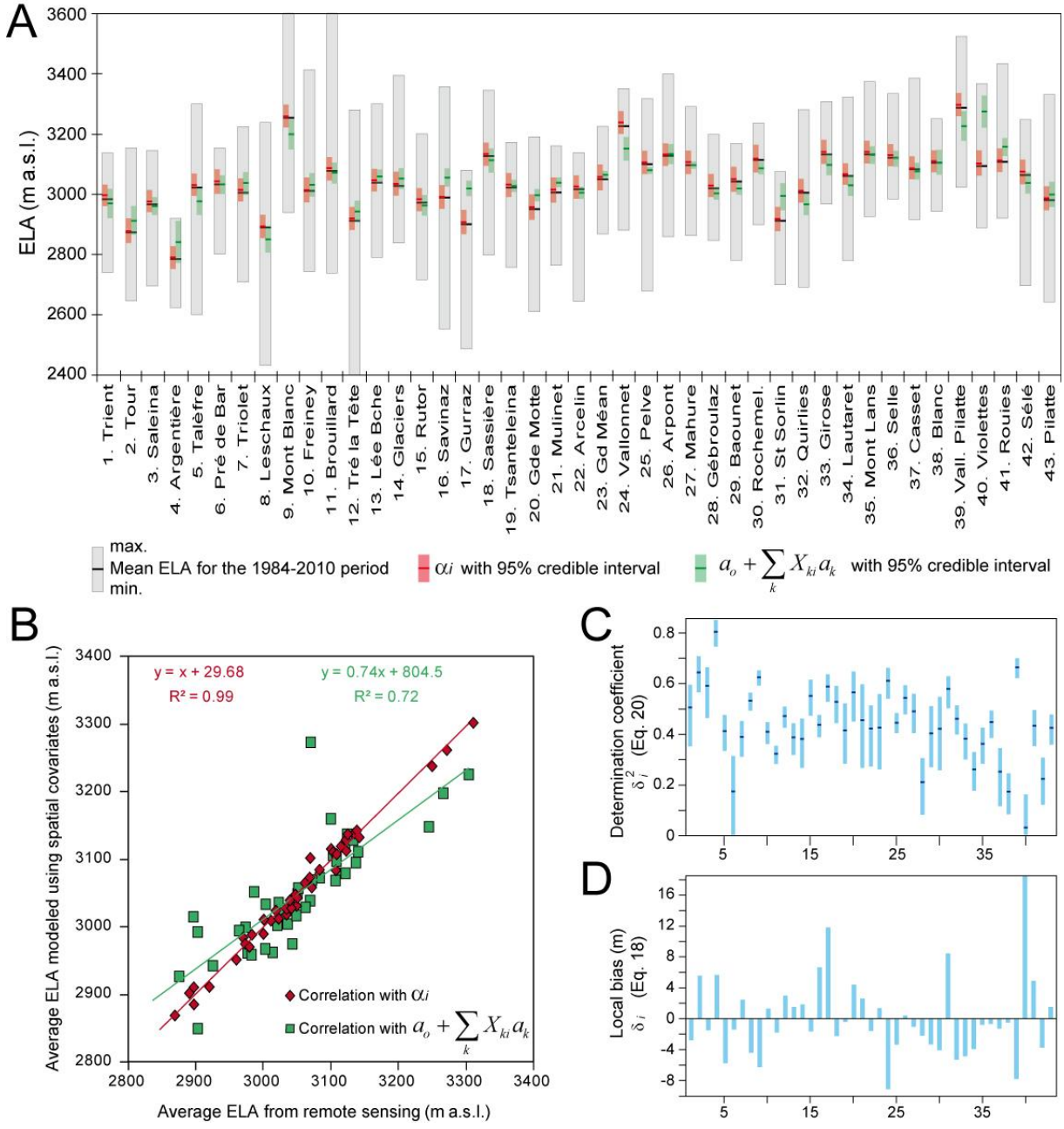

Supplementary material

Table I: Characteristics of the 122 satellite images used for SLA measurements. For Landsat images, the pixel size is 15 and 30 m for the panchromatic and multispectral modes respectively (LT5 = Landsat 5 TM, LE7 = Landsat 7 ETM+). For SPOT images the pixel size is 2.5, 5 or 10 m for the panchromatic mode (P) and 10 or 20 m for the multispectral mode (XS) depending on the satellite. For ASTER images the pixel size is 15 m.

Date	Sensor	Path-Row
31/08/1984	LT5	196-028 and 196-029
09/09/1984	LT5	195-028 and 195-029
02/08/1985	LT5	196-028 and 196-029
11/08/1985	LT5	195-028 and 195-029
28/09/1985	LT5	195-029
09/09/1986	LT5	196-028
05/10/1986	SPOT 1 P	051-258 and 051-259
17/10/1986	LT5	195-028
09/09/1987	LT5	196-028
18/09/1987	LT5	195-029
27/08/1988	LT5	195-028 and 195-029
12/09/1988	LT4	195-028 and 195-029
26/09/1988	SPOT-1 XS	050-259
30/07/1989	SPOT-1 P	051-259
13/08/1989	LT5	195-029
20/09/1989	SPOT-1 P	052-257 and 052-258
01/09/1990	SPOT-2 XS	051-259
10/09/1990	LT5	195-028
19/08/1991	LT5	196-029
25/08/1991	SPOT-2 P	052-257
30/08/1991	SPOT-2 P	051-258 and 051-259
05/08/1992	LT5	196-028
17/09/1992	SPOT-1 XS	051-259
21/09/1992	SPOT-1 XS	051-257 and 051-258
26 07 1993	SPOT-1 XS	050-259
02 09 1993	SPOT-2 XS	051-257
09/08/1994	SPOT-3 P	052-257 and 051-259
15/08/1994	SPOT-3 P	050-259 and 052-259
31/08/1995	SPOT-2 XS	051-259
31/07/1996	SPOT-3 P	052-259
08/08/1996	SPOT-2 XS	051-257
30/09/1997	SPOT-1 XS	051-257, 051-258, 051-259 and 051-260
26/08/1998	SPOT-4 XS	052-257
30/08/1998	SPOT-4 XS	051-259 and 052-258
02/09/1999	LE7	196-029
11/09/1999	LE7	195-028 and 195-029
12/08/2000	LE7	195-028
26/08/2000	SPOT-1 XS	051-257
28/08/2000	LE7	195-029
24/08/2001	SPOT-2 XS	050-259
29/08/2001	SPOT-1 XS	051-257
07/09/2001	ASTER-1	195-029
02/10/2001	LE7	195-028 and 195-029
02/08/2002	LE7	195-029
18/08/2002	LE7	195-028
14/09/2002	SPOT-5 XS	051-258
05/10/2002	LE7	195-028 and 195-029
12/08/2003	ASTER	195-029
13/08/2003	LT5	195-028 and 195-029
22/08/2003	SPOT-2 P	052-259
23/08/2003	SPOT-5 P	051-257 and 051-259
21/09/2003	LT5	196-029
14/08/2004	ASTER	195-029
27/08/2004	SPOT-5 XS	051-259
08/09/2004	LE7	195-028 and 195-029
08/09/2004	ASTER	195-028 and 195-029
01/08/2005	ASTER	195-027 and 195-028
10/08/2005	LE7	195-028
02/09/2005	LE7	196-028 and 196-029
05/09/2006	LE7	196-028 and 196-029
21/09/2006	LE7	196-028 and 196-029
16/10/2006	LE7	195-028 and 195-029
31/07/2007	LE7	195-028 and 195-029
24/09/2007	LE7	196-028 and 196-029
19/10/2007	LE7	195-029
19/10/2007	ASTER	196-028 and 196-029
18/08/2008	LE7	195-028 and 195-029
02/09/2008	SPOT 5 XS	051-257, 052-258, 052-259 and 051-260
07/09/2008	SPOT 4 XS	051-259
15/08/2009	SPOT-5 XS	052-257 and 052-258
06/09/2009	LE7	195-029
22/09/2009	LE7	195-028 and 195-029
29/09/2009	LE7	196-029
30/09/2009	LT5	195-028
31/08/2010	LE7	196-028 and 196-029
09/09/2010	LE7	195-029
15/09/2010	SPOT-5 XS	052-258
16/09/2010	ASTER	195-027, 195-028 and 195-029
23/09/2010	SPOT-4 XS	050-259

Table II: ELA of each one of the 43 glaciers for each year of the 1984-2010 period. Underlined data are calculated using the bi-linear regression method detailed in section 2.2.3.

Year	Trient	Tour	Saleina	Argentière	Taléfre	Pré Bar	Trioletl	Leschaux	Mt Blanc	Freiney	Brouill.	Tré la T.	Née Blandes	Glac. Rutor	Savinaz	Gurraz	Sassière	Tsantel.	Gde Motte	Mulinet
1984	*2642*	*2561*	*2631*	2700	*2696*	2800	2709	*2581*	2943	2530	*2777*	2394	2842	*2685*	2715	2552	2480	2797	2756	2609	2763
1985	2742	2660	2695	2623	2599	*2743*	2720	2429	3111	*2761*	*2836*	*2641*	*2746*	*2745*	2752	2595	2656	2895	2781	*2725*	2871
1986	3127	3084	3067	2787	3213	3153	3112	2975	3342	3078	3066	2862	3099	3006	3065	3014	2917	3169	3035	2953	3073
1987	2842	2653	2861	2668	2735	2939	2935	2630	3127	2756	2737	2612	2869	2837	2849	2691	2804	2884	*2926*	2872	*2897*
1988	2954	2714	2928	2761	2996	3039	3048	2859	3263	*3015*	*3090*	2831	3056	3053	2824	2680	2549	3017	2984	2853	2930
1989	3021	2801	3019	2805	3103	*3092*	3157	2942	3293	3157	*3185*	3135	3150	3073	3044	3026	2959	3059	3026	2887	3077
1990	3113	3118	3144	2861	3204	3091	3224	3225	3368	3358	3365	3250	3286	3396	3125	3190	2978	3268	3165	3034	3116
1991	3040	*2855*	2969	2818	*2990*	2991	*2950*	2814	3172	2994	3096	2761	2913	*2980*	3114	3079	2970	3303	3127	3146	*3114*
1992	3027	2967	3056	2816	3109	*3136*	*3108*	2899	3528	*3153*	*3229*	3138	3238	3142	*3061*	3220	3079	*3236*	*3141*	*3049*	*3112*
1993	3041	2840	2997	2745	3209	3044	3026	3026	3236	*3056*	3033	2896	3148	2888	2966	*2962*	*2855*	*3106*	2929	*2919*	*2982*
1994	2965	2715	2910	2770	2918	3024	2932	2755	3157	2825	2870	*2810*	2831	2935	2875	2935	2901	3088	2941	2871	2925
1995	*2738*	*2612*	*2710*	*2674*	*2777*	*2781*	*2752*	*2640*	*3012*	*2767*	*2838*	*2656*	*2785*	*2767*	*2773*	*2804*	*2697*	*2948*	*2853*	*2761*	*2823*
1996	2956	2701	2879	2732	2962	3014	2965	2728	*3165*	*2959*	*3034*	*2838*	*2944*	*2943*	*2850*	*2881*	*2774*	*3025*	*2930*	*2838*	*2900*
1997	3012	2810	2956	2747	3035	3052	3016	2805	*3238*	2968	3042	2946	3183	3036	2904	3051	2952	3176	*3041*	2961	*3012*
1998	3090	3099	3051	2834	3167	3074	3106	3237	3504	3306	3476	3143	3082	3093	3072	3044	2951	3235	3148	3156	3090
1999	2947	2768	2972	2740	2978	*2928*	*2900*	2892	3287	2823	2851	2794	2807	2953	2881	3015	2967	3037	3051	2878	3029
2000	2971	2815	2943	2843	2909	3034	2973	2948	3126	2933	2964	2672	2910	3000	2891	3043	2921	3175	3064	2923	3048
2001	2900	2707	2871	2665	2905	3034	2881	2594	2938	2745	2824	2664	2789	2917	2813	2595	2626	*2892*	2998	*2797*	*2704*	*2767*
2002	2903	2785	2926	2754	2965	3031	2993	2741	2937	2787	2796	2708	2861	2879	2880	3004	2822	2998	3020	2868	2950
2003	3110	3153	3112	2894	3167	3140	3089	3180	3550	3417	3609	3235	3313	3150	3202	3352	3086	3281	3162	3187	3159
2004	3068	3044	3068	2851	3157	3132	3075	3174	3498	3415	3596	3275	3287	3170	3108	3216	2995	3341	3173	3134	3098
2005	3067	3046	3134	2866	3141	3092	3038	3165	3269	3080	3042	3213	3163	3125	3186	3204	2990	3307	*3175*	3048	3095
2006	3063	2869	3028	2840	3055	*3071*	*3042*	2966	3399	3082	3048	2924	3131	3114	*3007*	2968	2952	*3182*	*3087*	*2995*	*3058*
2007	3018	2708	2934	2765	3043	3044	3000	2749	3278	2840	3074	2781	2891	3079	2905	2972	2930	3179	2985	2882	2986
2008	3056	2975	3062	2855	3117	3037	3001	2964	3211	3016	2991	2917	3085	3013	3117	3136	3007	3258	3139	2997	3041
2009	3133	3139	3116	2914	3299	3145	3103	3052	3616	3394	3599	3273	3258	3325	3045	3045	3036	3281	3076	3080	3075
2010	2892	2832	2854	2770	3029	2935	2959	2811	3249	3004	3047	2842	3034	2914	3117	3030	2972	3190	3115	2930	3071

Year	Arcelin	Gd Méan	Pelve	Vallonn	Arpont	Mahure	Gébroul	Baoune	Rochem.	St Sorlin	Quirlies	Girose	Lautaret	Mt de L.	Selle	Casset	Blanc	Val. Pilat	Violett.	Rouies	Sélé	Pilatte
1984	2643	2878	2683	2879	2951	2864	2927	2780	2900	2784	2755	3065	3016	3042	3007	2979	3016	3022	3052	2922	2953	2868
1985	*2783*	2894	2678	3162	2852	*2899*	2973	2816	2985	2870	2847	3089	3043	3119	3030	3043	3091	3299	3072	3019	3098	2887
1986	3096	3068	3143	3262	3164	3141	3014	3015	*3151*	3074	2936	*3209*	3096	*3183*	3170	3060	3160	3469	*3133*	3184	3145	*3034*
1987	3008	*2958*	2852	3287	3109	2976	2985	*2954*	*3012*	2905	2804	3099	3043	3093	3020	3051	3063	3179	*3005*	2999	3040	2895
1988	3007	3022	2757	3282	2949	2880	2954	3013	3043	2849	2782	3085	3014	3100	3024	3031	3039	3318	3021	2930	2978	2789
1989	3096	3064	3209	3303	*3176*	*3156*	3081	*3102*	*3160*	3165	2919	3300	3220	3226	3267	3149	3164	3521	3204	3143	3151	3219
1990	3109	3172	3246	3346	3399	*3247*	3095	3140	*3251*	2983	2920	3102	3055	3054	3086	3085	3036	3154	3065	3041	3058	3062
1991	3124	*3175*	3284	*3333*	3127	3209	3027	*3171*	*3229*	3018	2858	3141	3034	3159	3167	3070	3146	3290	3032	3063	3126	2887
1992	3076	*3173*	3170	*3331*	3220	3159	3076	*3169*	*3227*	3059	2935	3094	3109	3084	3171	3067	3162	3278	3077	*3091*	*3086*	*2984*
1993	*2977*	*3042*	3187	3286	3151	2977	2942	*3039*	*3097*	*3011*	*2891*	3117	3050	3076	3152	3042	3108	*3276*	*3056*	*3065*	*3060*	*2958*
1994	3007	2991	3129	3253	3054	3068	2941	3004	3047	2836	2769	3068	3048	3091	3004	3056	3016	3264	3053	*3008*	*3003*	*2901*
1995	*2818*	*2884*	*2932*	*3043*	2902	2858	2825	*2881*	*2939*	2689	2698	3026	2978	3091	2989	2996	3028	3032	*2943*	2997	3037	2884
1996	2928	*2961*	2951	3138	2929	3037	2977	2992	3006	*2878*	*2758*	3002	2935	*2974*	2983	2913	2942	*3143*	*2924*	*2932*	*2927*	*2825*
1997	3050	*3073*	3126	3245	3113	3000	3000	*3069*	*3127*	2860	2890	3083	3057	2981	3027	3035	3037	3245	3039	3022	3006	2860
1998	3117	3194	3274	3290	3283	3165	3084	3142	3214	3173	2977	3190	3118	3163	3185	3112	3137	3452	3209	*3159*	*3154*	*3052*
1999	3036	3043	3204	3281	3105	3130	2990	3101	3155	2970	2863	3129	2990	3105	2982	3080	3086	3242	3028	3001	3018	2888
2000	3058	3090	3162	3288	3113	3136	3004	3047	3189	3034	2898	3169	3046	3112	3044	3100	3152	3267	3073	3030	3084	2903
2001	*2762*	*2828*	*2876*	*2987*	2879	*2878*	2848	2852	*2882*	2780	2750	3073	2779	3017	2982	*2894*	3001	*3107*	3022	2922	2701	2644
2002	2938	2923	3097	3108	2992	2998	2988	3001	3014	3107	3059	3066	3028	2925	3141	3035	3085	3159	3038	3020	3070	2810
2003	3123	3230	3317	3320	3356	3268	3193	3134	3182	3280	3074	3307	3319	3369	3333	3242	3230	3428	3366	3435	3249	3334
2004	3117	3192	3281	3348	3281	3273	3077	3156	3166	3219	2986	3290	3146	3313	3237	3183	3169	3452	3068	3373	3175	3047
2005	3128	3176	3297	3297	3330	3274	3108	3167	*3261*	3229	3041	3256	3234	3342	3227	3381	3250	*3478*	*3258*	3432	3153	3207
2006	3054	*3119*	3195	*3277*	3213	3199	3041	*3115*	*3173*	3060	2968	3252	3104	3220	3227	*3163*	3189	3440	3059	3208	3096	3174
2007	3018	3044	3149	3279	3168	3101	3010	3122	3194	3194	2981	3161	3033	3104	3264	3109	3167	3460	3087	3185	3134	3122
2008	3079	3063	3262	3300	*3225*	3186	3063	3124	3216	3010	2831	2967	2999	3085	3017	3057	3058	3324	*3022*	3048	2994	2998
2009	3127	3121	3303	3304	3169	3288	3138	3178	3235	3241	3056	3296	3156	3304	3307	3158	3166	3424	3063	3147	3160	3153
2010	2875	3126	3071	3124	3274	3284	3037	3132	3167	2939	2958	3120	3018	*3082*	3215	3037	3070	3267	2888	3065	3084	2803